BOLD and EEG Signal Variability at Rest Differently Relate to Aging in the Human Brain

D. Kumral[1,2], F. Şansal[3,1], E. Cesnaite[1], K. Mahjoory[1,4], E. Al[2,1], M. Gaebler[1,2], V. V. Nikulin[1,5,6], A. Villringer[1,2,7,8]

[1]Department of Neurology, Max Planck Institute for Human Cognitive and Brain Sciences, Leipzig, Germany
[2]MindBrainBody Institute at the Berlin School of Mind and Brain, Humboldt-Universität zu Berlin, Berlin, Germany
[3]International Graduate Program Medical Neurosciences, Charité-Universitätsmedizin, Berlin, Germany
[4]Institute for Biomagnetism and Biosignalanalysis, University of Muenster, Muenster, Germany
[5]Neurophysics Group, Department of Neurology, Campus Benjamin Franklin, Charité Universitätsmedizin Berlin, Berlin, Germany
[6]Centre for Cognition and Decision Making, National Research University Higher School of Economics, Moscow, Russian Federation
[7]Center for Stroke Research Berlin, Charité – Universitätsmedizin Berlin, Berlin, Germany
[8]Department of Cognitive Neurology, University Hospital Leipzig

Corresponding author: Deniz Kumral, Department of Neurology, Max Planck Institute for Human Cognitive and Brain Sciences, Stephanstrasse 1A, 04103, Leipzig, Germany.
Email: dkumral@cbs.mpg.de

Abbreviations: BOLD – Blood Oxygenation Level Dependent; CBF – cerebral blood flow; CBV– cerebral blood volume; CCA – canonical correlation analysis; $CMRO^2$ – cerebral metabolic rate of oxygen; CVR – cerebrovascular reactivity; DMN – Default Mode Network; EEG – electroencephalography; EC – eyes closed; EO – eyes open; FDR - false discovery rate; FEM – finite element method; fMRI – functional Magnetic Resonance Imaging; fNIRS – functional Near-Infrared Spectroscopy; FWHM – full-width half-maximum; ICBM – International Consortium for Brain Mapping; MEG – magnetoencephalography; MNI – Montreal Neurological Institute; rho – Spearman's rank correlation coefficient; PET –Positron-emission tomography; ROI – regions of interests; rs – resting state; SD – standard deviation; SVD – Singular Value Decomposition

Abstract

Variability of neural activity is regarded as a crucial feature of healthy brain function, and several neuroimaging approaches have been employed to assess it noninvasively. Studies on the variability of both evoked brain response and spontaneous brain signals have shown remarkable changes with aging but it is unclear if the different measures of brain signal variability – identified with either hemodynamic or electrophysiological methods – reflect the same underlying physiology. In this study, we aimed to explore age differences of spontaneous brain signal variability with two different imaging modalities (EEG, fMRI) in healthy younger (25±3 years, N=135) and older (67±4 years, N=54) adults. Consistent with the previous studies, we found lower blood oxygenation level dependent (BOLD) variability in the older subjects as well as less signal variability in the amplitude of low-frequency oscillations (1–12 Hz), measured in source space. These age-related reductions were mostly observed in the areas that overlap with the default mode network. Moreover, age-related increases of variability in the amplitude of beta-band frequency EEG oscillations (15–25 Hz) were seen predominantly in fronto-temporal and sensorimotor brain regions. There were significant sex differences in BOLD and EEG signal variability in various brain regions, but no significant interactions between age and sex were observed. Further, both univariate and multivariate correlation analyses revealed no significant associations between these two variability measures. In summary, we show that both BOLD and EEG signal variability reflect aging-related processes but are likely to be dominated by different physiological origins, which relate differentially to age and sex.

Keywords: brain signal variability, resting state, BOLD, fMRI, EEG, aging, sex, default mode network

1. Introduction

Functional neuroimaging methods such as fMRI, PET, fNIRS, EEG, or MEG have allowed the non-invasive assessment of functional changes in the aging human brain (Cabeza, 2001; Cabeza et al., 2018). Most previous functional neuroimaging studies on aging have employed a task-based design (Grady, 2012) and in their data analysis the central tendency has typically been assumed to be the most representative value in a distribution (e.g., mean) (Speelman and McGann, 2013) or the "signal" within distributional "noise". In recent years, also the variability of brain activation in task-dependent and task-independent measurements (as spontaneous variations of background activity) has been shown to provide relevant information about the brain's functional state (Garrett et al., 2013b; Grady and Garrett, 2018; Nomi et al., 2017). These studies primarily measured the blood oxygen level dependent (BOLD) signal using fMRI. For example, it has been demonstrated that the variance of the task-evoked BOLD response was differentially related to aging as well as cognitive performance (Armbruster-Genc et al., 2016; Garrett et al., 2013a). Similarly, spontaneous signal variability in resting state fMRI (rsfMRI) has been associated with age (Grady and Garrett, 2018; Nomi et al., 2017), emotional state (state anxiety; Labrenz et al., 2018), and mental or neural disorders such as stroke (Kielar et al., 2016), Attention Deficit Hyperactivity Disorder (Nomi et al., 2018) or 22q11.2 deletion syndrome (Zöller et al., 2017). From these studies, it was concluded that reductions in BOLD signal variability might serve as an index for deficits in neural processing and cognitive flexibility (Grady and Garrett, 2014).

These conclusions of aforementioned studies imply that BOLD signal variability is mainly determined by *neuronal* variability. To a large extent, this is based on the premise that BOLD is related to neuronal activity: The evoked BOLD signal in task-based fMRI reflects the decrease of the deoxyhemoglobin concentration to changes in local brain activity, which is determined by vascular (blood velocity and volume: "neurovascular coupling") and metabolic (oxygen consumption: "neurometabolic coupling") factors (Logothetis and Wandell, 2004; Villringer and Dirnagl, 1995). The BOLD signal is therefore only an indirect measure of neural activity (Logothetis, 2008). For the variability of task-evoked BOLD signal and for spontaneous variations of the BOLD signal, in principle, the same considerations apply regarding their relationship to underlying neural processes (Murayama et al., 2010). However, since in rsfMRI there is no explicit external trigger for evoked brain activity to which time-locked averaging could be applied, the time course of rsfMRI signals is potentially more susceptible to contributions of "physiological noise", such as cardiac and respiratory signals (Birn et al., 2008; Chang et al., 2009), but also spontaneous fluctuations of vascular tone,

which is found even in isolated arterial vessels (Failla et al., 1999; Hudetz et al., 1998; Wang et al., 2006). In the same vein, the variability of task-evoked fMRI is not necessarily reflecting only the variability of evoked neuronal activity, as it may also – at least partly – reflect the variability of the spontaneous background signal on which a constant evoked response is superimposed.

In aging, non-neuronal signal fluctuations may also introduce spurious common variance across the rsfMRI time series (Caballero-Gaudes and Reynolds, 2017), thus confounding estimates of "neural" brain signal variability. Previous evidence suggests that the relationship between neuronal activity and the vascular response is attenuated with age – and so is, as a consequence, the BOLD signal (for review see D'Esposito et al., 2003). For instance, aging has been associated with altered cerebrovascular ultrastructure, reduced elasticity of vessels, and atherosclerosis (Farkas and Luiten, 2001) but also with a decrease in resting cerebral blood flow (CBF) (Ances et al., 2009; Martin et al., 1991), cerebral metabolic rate of oxygen consumption ($CMRO^2$) (Aanerud et al., 2012), and cerebrovascular reactivity (CVR) (Liu et al., 2013). Taken together, age-related changes in BOLD signal or BOLD signal variability are related to a mixture of alterations in non-neural spontaneous fluctuations of vascular signals, neural activity, neurovascular coupling, and/or neurometabolic coupling (D'Esposito et al., 2003; Geerligs et al., 2017; Tsvetanov et al., 2015).

While BOLD fMRI signal and specifically variance measures based on fMRI are only partially and indirectly related to neural activity (Liu, 2013; Logothetis, 2008), electrophysiological methods such as EEG can provide a more direct assessment of neural activity with a higher temporal but poorer spatial resolution (Cohen, 2017). EEG measures neuronal currents resulting from the synchronization of dendritic postsynaptic potentials across the neural population; the cerebral EEG rhythms thereby reflect the underlying brain neural network activity (Steriade, 2006). Resting state (rs)EEG is characterized by spontaneous oscillations ("brain rhythms") at different frequencies. Previously, the mean amplitude of low-frequency bands (e.g., delta and/or theta, 1-7 Hz) has been shown to correlate negatively with age (Vlahou et al., 2015), while higher-frequency bands (e.g., beta, 15-25 Hz) show the reverse pattern (Rossiter et al., 2014). However, less is known about the within-subject variability of EEG measures and their association with aging. Several studies have addressed the variability in the spectral amplitudes of different frequency bands using variance (Hawkes and Prescott, 1973; Oken and Chiappa, 1988), coefficient of variation (Burgess and Gruzelier, 1993; Maltez et al., 2004), and complexity (Fernández et al., 2012; Sleimen-Malkoun et al., 2015). For instance, reductions of the complexity in rsEEG signal

have been found not only in healthy aging (Yang et al., 2013; Zappasodi et al., 2015) but also in age-related pathologies such as mild cognitive impairment (McBride et al., 2014) and Alzheimer's disease (Smits et al., 2016). Accordingly, it has been suggested that irregular (e.g., variable) systems indicate a normal and healthy state (more integrated information) while highly regular systems often mark dysfunction or disease (Lipsitz and Goldberger, 1992; Vaillancourt and Newell, 2002).

The different methodological approaches, fMRI based "vascular" approaches on the one hand and electrophysiological methods such as EEG and MEG, on the other hand, indicate alterations of brain signal variability with aging. However, it remains unclear whether these different measures of brain variability at rest reflect the same underlying physiological changes. Evidently, there are some correlations between the two signal sources (for a review see, Jorge et al., 2014; Ritter and Villringer, 2006). For instance, in task-based EEG-fMRI simultaneous recordings, a relationship between BOLD responses and amplitude of evoked potentials has been demonstrated (e.g., Ritter et al., 2009; Seaquist et al., 2007), while in resting state EEG-fMRI studies, a negative association between spontaneous modulations of alpha rhythm and BOLD signal has also been established (e.g., Chang et al., 2013; Goldman et al., 2002; Gonçalves et al., 2006; Moosmann et al., 2003). Further, differential correlation patterns have been noted for the various rhythms of different frequencies in EEG/MEG and the fMRI signal, such that low-frequency oscillations show a negative (Deligianni et al., 2014; Mantini et al., 2007; Meyer et al., 2013), while higher frequencies oscillations demonstrate a positive correlation with the BOLD signal (Niessing et al., 2005; Scheeringa et al., 2011).

Regarding the known age-related changes in BOLD and EEG signal variability, respectively, the question arises whether these alterations are dominated by joint signal sources of fMRI and EEG or by – potentially different – signal contributions that relate to each of these two methods. Given the – potentially large – non-neuronal signal contribution, this issue is particularly relevant for rsfMRI studies. Here, we addressed this question analyzing rsfMRI and EEG measures of variability in healthy younger and older subjects. To our knowledge, the only study that compared variability in a "vascular" imaging method (rsfMRI) and an electrophysiological method (rsMEG at the sensor space) concluded that the effects of aging on BOLD signal variability were mainly driven by vascular factors (e.g., heart rate variability) and not well-explained by the changes in neural variability (Tsvetanov et al., 2015). The main aims of the present study were to explore i) age differences of brain signal variability measures, as well as to investigate ii) how neural variability derived from rsEEG related to the analogous parameters of BOLD signal variability derived from rsfMRI.

We used rsfMRI and rsEEG from the "Leipzig Study for Mind-Body-Emotion Interactions" (Babayan et al., 2019). As an explanatory analysis, we further investigated sex-related differences of brain signal variability measures. To measure the brain signal variability, we calculated the standard deviation (SD) of both the BOLD signal and of the amplitude envelope of the filtered rsEEG time series for a number of standard frequency bands at the source space. We hypothesized that brain signal variability would generally decrease with aging. In addition, based on the premise that BOLD fMRI signal variability reflects *neural* variability as measured by rsEEG, we expected that the corresponding changes in both signal modalities would demonstrate moderate to strong similarity in their spatial distribution. Given the confounding effects of vascular factors during aging on the fMRI signal (D'Esposito et al., 2003; Liu, 2013; Thompson, 2018), we further expected to find the relationship between BOLD and EEG signal variability to be stronger in younger than older adults.

2. Method

2.1.Participants

The data of the "Leipzig Study for Mind-Body-Emotion Interactions" (LEMON; Babayan et al., 2019) comprised 227 subjects in two age groups (younger: 20-35, older: 59-77). Only participants who did not report any neurological disorders, head injury, alcohol or other substance abuse, hypertension, pregnancy, claustrophobia, chemotherapy and malignant diseases, current and/or previous psychiatric disease or any medication affecting the cardiovascular and/or central nervous system in a telephone pre-screening were invited to the laboratory. The study protocol conformed to the Declaration of Helsinki and was approved by the ethics committee at the medical faculty of the University of Leipzig (reference number 154/13-ff).

RsEEG recordings were available for 216 subjects who completed the full study protocol. We excluded data from subjects that had missing event information (N=1), different sampling rate (N=3), mismatching header files or insufficient data quality (N=9). Based on the rsfMRI quality assessment, we further excluded data from subjects with faulty preprocessing (N=7), ghost artefacts (N=2), incomplete data (N=1), or excessive head motion (N=3) (criterion: mean framewise displacement (FD) ≤ 0.5 mm; Power et al., 2012) (Supplementary Figure 1). The final sample included 135 younger ($M = 25.10 \pm 3.70$ years, 42 females) and 54 older subjects ($M = 67.15 \pm 4.52$ years, 27 females).

2.1.fMRI Acquisition

Brain imaging was performed on a 3T Siemens Magnetom Verio MR scanner (Siemens Medical Systems, Erlangen, Germany) with a standard 32-channel head coil. The participants were instructed to keep their eyes open and not fall asleep.

The structural image was recorded using an MP2RAGE sequence (Marques et al., 2010) with the following parameters: TI 1 = 700 ms, TI 2 = 2500 ms, TR = 5000 ms, TE = 2.92 ms, FA 1 = 4°, FA 2 = 5°, band width = 240 Hz/pixel, FOV = 256 × 240 × 176 mm^3, voxel size = 1 x 1 x 1 mm^3. The functional images were acquired using a T2*-weighted multiband EPI sequence with the following parameters: TR = 1400 ms, TE = 30 ms, FA= 69°, FOV = 202 mm, voxel size = 2.3 x 2.3 x 2.3 mm^3, slice thickness = 2.3 mm, slice gap = 0.67 mm, 657 volumes, multiband acceleration factor = 4, duration = 15 min 30 s. A gradient echo field map with the sample geometry was used for distortion correction (TR = 680 ms, TE 1 = 5.19 ms, TE 2 = 7.65 ms).

2.2.fMRI Preprocessing

Preprocessing was implemented in Nipype (Gorgolewski et al., 2011), incorporating tools from FreeSurfer (Fischl, 2012), FSL (Jenkinson et al., 2012), AFNI (Cox, 1996), ANTs (Avants et al., 2011), CBS Tools (Bazin et al., 2014), and Nitime (Rokem et al., 2009). The pipeline comprised the following steps: (I) discarding the first five EPI volumes to allow for signal equilibration and steady state, (II) 3D motion correction (FSL mcflirt), (III) distortion correction (FSL fugue), (IV) rigid body coregistration of functional scans to the individual T1-weighted image (Freesurfer bbregister), (V) denoising including removal of 24 motion parameters (CPAC, Friston et al., 1996), motion, signal intensity spikes (Nipype rapidart), physiological noise in white matter and cerebrospinal fluid (CSF) (CompCor; Behzadi et al., 2007), together with linear and quadratic signal trends, (VI) band-pass filtering between 0.01-0.1 Hz (Nilearn), (VII) spatial normalization to MNI152 (Montreal Neurological Institute) standard space (2 mm isotropic) via transformation parameters derived during structural preprocessing (ANTS). (VIII) The data were then spatially smoothed with a 6-mm full-width half-maximum (FWHM) Gaussian kernel.

BOLD Signal Variability (SD_{BOLD}). Standard deviation (SD) quantifies the amount of variation or dispersion in a set of values (Garrett et al., 2015; Grady and Garrett, 2018). Higher SD in rsfMRI signal indicates greater intensity of signal fluctuation or an increased level of activation in a given area (Garrett et al., 2011). We first calculated SD_{BOLD} across the whole time series for each voxel and then within 96 boundaries of preselected atlas-based regions of interests (ROIs) based on the Harvard-Oxford cortical atlas (Desikan et al., 2006). The main steps of deriving brain signal variability (SD_{BOLD}) from the preprocessed fMRI signal are shown in Figure 1.

The reproducible workflows containing fMRI preprocessing details can be found here: https://github.com/NeuroanatomyAndConnectivity/pipelines/releases/tag/v2.0.

2.3.EEG Recordings

Sixteen minutes of rsEEG were acquired on a separate day with BrainAmp MR-plus amplifiers using 61 ActiCAP electrodes (both Brain Products, Germany) attached according to the international standard 10-20 localization system (Jurcak et al., 2007) with FCz as a reference. The ground electrode was located at the sternum. Electrode impedance was kept below 5 kΩ. Continuous EEG activity was digitized at a sampling rate of 2500 Hz and band–pass filtered online between 0.015 Hz and 1 kHz.

The experimental session was divided into 16 blocks, each lasting 60 s, with two conditions interleaved, eyes closed (EC) and eyes open (EO), starting with the EC condition. Changes between blocks were announced with the software Presentation (v16.5, Neurobehavioral Systems Inc., USA). Participants were asked to sit comfortably in a chair in a dimly illuminated, sound-shielded Faraday recording room. During the EO periods, participants were instructed to stay awake while fixating a black cross presented on a white background. To maximize comparability, only EEG data from the EO condition were analyzed, since rsfMRI data were collected only in the EO condition.

2.4.EEG Data Analysis

EEG processing and analyses were performed with custom Matlab (The MathWorks, Inc, Natick, Massachusetts, USA) scripts using functions from the EEGLAB environment (version 14.1.1b; Delorme and Makeig, 2004). The continuous EEG data were down-sampled to 250 Hz, band-pass filtered within 1–45 Hz (4^{th} order back and forth Butterworth filter) and split into EO and EC conditions. Segments contaminated by large artefacts due to facial muscle tensions and gross movements were removed following visual inspection; rare occasions of artifactual channels were excluded from the analysis. The dimensionality of the data was reduced using principal component analysis (PCA) by selecting at least 30 principle components explaining 95% of the total variance. Next, using independent component analysis (Infomax; Bell and Sejnowski, 1995), the confounding sources e.g. eye-movements, eye-blinks, muscle activity, and residual ballistocardiographic artefacts were rejected from the data.

2.5.EEG Source Reconstruction

Before conducting source reconstruction, preprocessed EEG signals were re-referenced to a common average. We incorporated a standard highly detailed finite element method (FEM) volume conduction model as described by Huang et al. (2016).
The geometry of the FEM model was based on an extended MNI/ICBM152 (International Consortium for Brain Mapping) standard anatomy, where the source space constrained to cortical surface and parceled to 96 ROIs based on the Harvard-Oxford atlas (Desikan et al., 2006). The forward model was also expressed in MNI coordinates and determined using boundary element models as implemented in the M/EEG Toolbox of Hamburg (METH; Haufe and Ewald, 2016; Huang et al., 2016). The leadfield matrix was calculated between 1804 points located on the cortical surface to the 61 scalp electrodes. Source activity was

estimated using exact low-resolution tomography (eLORETA; Haufe and Ewald, 2016; Pascual-Marqui, 2007). Following the singular value decomposition (SVD) of each voxel's three-dimensional time course, the dominant orientation of the source signal was identified by preserving the first SVD component. We filtered into several frequency bands, associated with brain oscillations: delta (1–3 Hz), theta (4–8 Hz), alpha (8–12 Hz), and beta (15–25 Hz). The amplitude envelope of filtered oscillations was extracted using the Hilbert transform. Next, we applied temporal coarse graining by averaging data points in non-overlapping windows of length 0.5 s (Figure 1).

EEG Variability (SD_{EEG}). We calculated the SD of amplitude envelope of band-pass filtered oscillations on the coarse-grained signal. RsEEG signal variability (SD_{EEG}) was obtained for different frequency bands (SD_{DELTA}, SD_{THETA}, SD_{ALPHA}, SD_{BETA}) in each of 96 ROIs. Main steps toward deriving brain signal variability from the preprocessed EEG signal are shown in Figure 1. The raw and preprocessed fMRI and EEG data samples can be found at https://ftp.gwdg.de/pub/misc/MPI-Leipzig_Mind-Brain-Body-LEMON/

Figure 1. Main steps of deriving brain signal variability from the preprocessed resting state fMRI and EEG signal. We calculated the standard deviation of the blood oxygen level dependent (BOLD) signal and of the coarse-grained amplitude envelope of the rsEEG time series for a number of standard frequency bands at the source space.

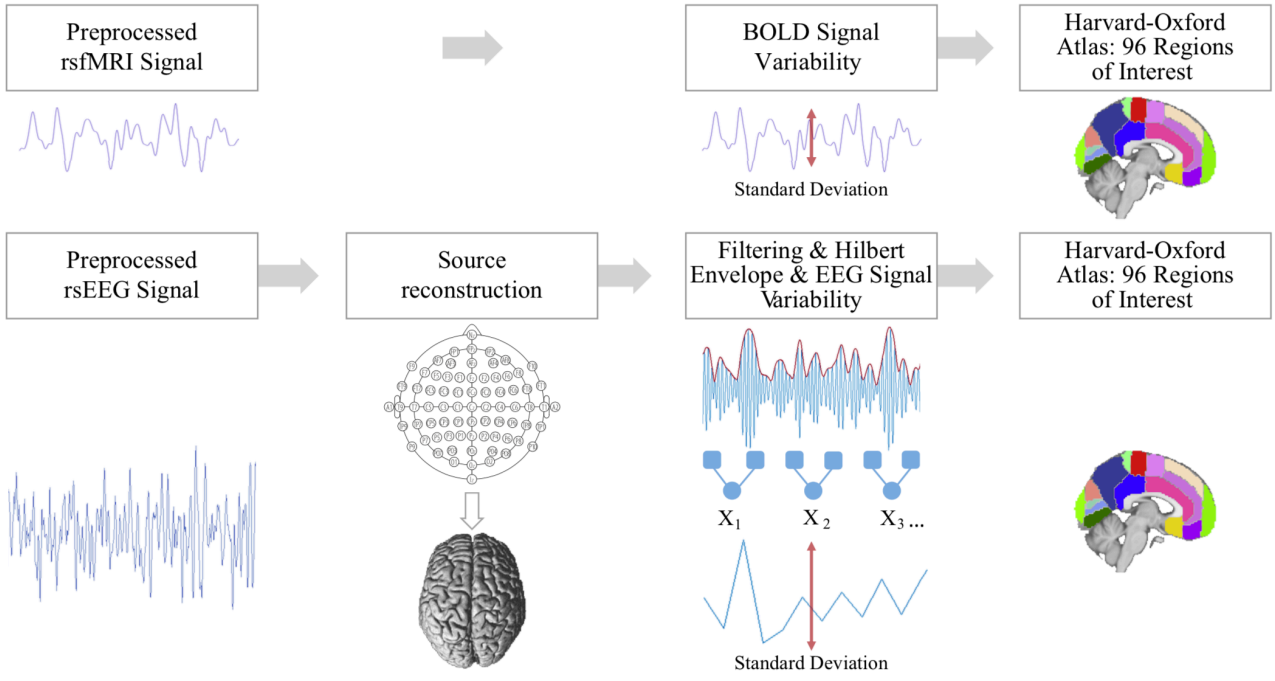

2.6.Statistical Analyses

Mean SD_{BOLD} and SD_{EEG}. For the topographic information (based on ROIs), the mean BOLD and EEG variability were calculated by I) log-transforming the SD values, II) averaging separately for younger and older subjects, and III) back-transforming then the values (McDonald, 2014).

Age and Sex Effects. A series of 2x2 (age group vs. sex) analyses of variance (ANOVAs) were applied to each ROI of brain signal variability values separately for SD_{BOLD} and SD_{EEG}, using controlling false discovery rate (FDR) according to Benjamini and Hochberg (1995) as correction for multiple comparisons. Significant group differences were further examined by Tukey HSD post-hoc comparisons.

The signal variability values were log-transformed to normalize SD_{BOLD} and SD_{EEG} before further analyses (assessed by Lilliefors test at a significance level of 0.05). Analyses were performed using R (R core team, 2018).

SD_{BOLD} – SD_{EEG} Correlation. To investigate the association between each ROI of SD_{BOLD} and SD_{EEG}, we used pairwise Spearman's rank correlation separately for younger and older subjects, corrected for FDR (96 ROIs). We further applied sparse canonical correlation analysis (CCA) to show that the relationship between SD_{BOLD} and SD_{EEG} is not missed when only mass bivariate correlations are used. CCA is a multivariate method to find the independent linear combinations of variables such that the correlation between variables is maximized (Witten et al., 2009). The sparse CCA criterion is obtained by adding a Lasso Penalty function (l_1), which performs continuous shrinkage and automatic variable selection and can solve statistical problems such as multicollinearity and overfitting (Tibshirani, 2011). We used l_1 penalty as the regularization function to obtain sparse coefficients, that is, the canonical vectors (i.e., translating from full variables to a data matrix's low-rank components of variation) will contain exactly zero elements. Sparse CCA was performed using the R package PMA (Penalized Multivariate Analysis; Witten et al., 2009; http://cran.r-project.org/web/packages/PMA/). In our analyses, the significance of the correlation was estimated using the permutation approach (N=1000) as implemented in the CCA.permute function in R ($p_{perm}<0.05$).

3. Results

Mean SD_{BOLD} and SD_{EEG}. The topographic distribution of SD_{BOLD} in younger adults revealed the largest brain signal variability values in fronto-temporal regions while in older adults it was in the frontal and occipital areas. Further, we found strongest variability across younger subjects in occipito-temporal regions for SD_{DELTA}, SD_{THETA}, SD_{ALPHA}, and in medial frontal brain regions for SD_{BETA}, while older adults showed strongest brain signal variability in the fronto-central brain regions for SD_{DELTA}, in parietal-central brain regions for SD_{THETA}, SD_{ALPHA}, and in medial frontal brain regions for SD_{BETA}. The details of topographic distribution of SD_{BOLD} and SD_{EEG} across age groups are available at Neurovault (https://neurovault.org/collections/WWOKVUDV/).

Age and Sex Effects. The 2x2 ANOVA analyses with SD_{BOLD} as dependent variable demonstrated that there was a significant main effect of age group in 49 ROIs in frontal, temporal, and occipital brain regions (F-values: 13.01–63.25; Figure 2). We also found a significant main effect of sex on SD_{BOLD} in 17 ROIs, mainly in frontal and occipital brain regions (F-values: 13.19–32.04; Figure 3) but no significant interaction between age group and sex (all $p_{FDR}>0.05$). Tukey HSD post-hoc analyses showed that older subjects had decreased SD_{BOLD} compared to younger adults which were presented in both sexes ($n_{ROI}=31$, Supplementary Figure 3A). We further found that male subjects had higher SD_{BOLD}, that was restricted to the groups of younger adults in most of the significant ROIs ($n_{ROI}=12$, Supplementary Figure 3B).

The 2x2 ANOVAs with SD_{EEG} as dependent variable showed significant main effects of age group in all frequency bands: SD_{DELTA} in 17 ROIs in occipital and frontal lobes (F-values: 12.77–25.64), SD_{THETA} in 13 ROIs in frontal (F-values: 14.18–36.62), SD_{ALPHA} in 13 ROIs in occipital (F-values: 13.35–18.83), and SD_{BETA} in 63 ROIs in central, fronto-temporal, and sensorimotor brain regions (F-values: 12.71–38.71), as shown in Figure 2. There were also significant main effects of sex in all frequency bands: SD_{DELTA} in 9 ROIs in occipital (F-values: 12.57–19.17), SD_{THETA} in 46 ROIs in occipital and temporal (F-values: 12.51–25.95), SD_{ALPHA} in 4 ROIs in frontal (F-values: 12.69–17.40), and SD_{BETA} in 61 ROIs in temporal, occipital, and frontal (F-values: 12.73–46.91), as shown in Figure 3. No significant interaction effects between age group and sex on SD_{EEG} were observed in any frequency band ($p_{FDR}>0.05$). Tukey HSD post-hoc analyses on SD_{EEG} showed that older subjects had less brain signal variability, which was present in both sexes for SD_{DELTA} ($n_{ROI}=11$), SD_{THETA} ($n_{ROI}=10$), and SD_{ALPHA} ($n_{ROI}=11$). Additionally, older adults showed higher SD_{BETA}, driven by female subjects ($n_{ROI}=39$) (Supplementary Figure 3A). With regard

to sex differences, post-hoc analyses showed that females had higher SD_{DELTA}, SD_{THETA}, SD_{ALPHA}, and SD_{BETA} than males. The sex differences in SD_{DELTA} (n_{ROI}=8) were mostly pronounced in younger adults, while the effect of sex in SD_{THETA} (n_{ROI}=29) and SD_{BETA} (n_{ROI}=44) were mainly presented in both age groups ($p<0.05$) (Supplementary Figure 3B). The graphical distribution of the F-values for the main effects of age group or sex for each ROI are shown in Supplementary Figure 2. Additional tables and boxplots showing SD_{BOLD} and SD_{EEG} for each frequency band and in each the 96 ROIs, split up by age group and sex, are presented in the Supplementary Tables 1-5.

Figure 2. Spatial maps of significant age group differences in SD_{BOLD} and SD_{EEG}.
We calculated the standard deviation (SD) of the blood oxygen level dependent (BOLD) signal and of the coarse-grained amplitude envelope of the rsEEG time series for the delta (1–3 Hz), theta (4–8 Hz), alpha (8–12 Hz), and beta (15–25 Hz) frequency bands at the source space. Statistical significance was determined using 2x2 ANOVAs corrected for multiple comparisons by false discovery rates (FDR; Benjamini and Hochberg, 1995). Blue colored areas indicate where brain signal variability was lower in older than in younger adults, while red color indicates the opposite.

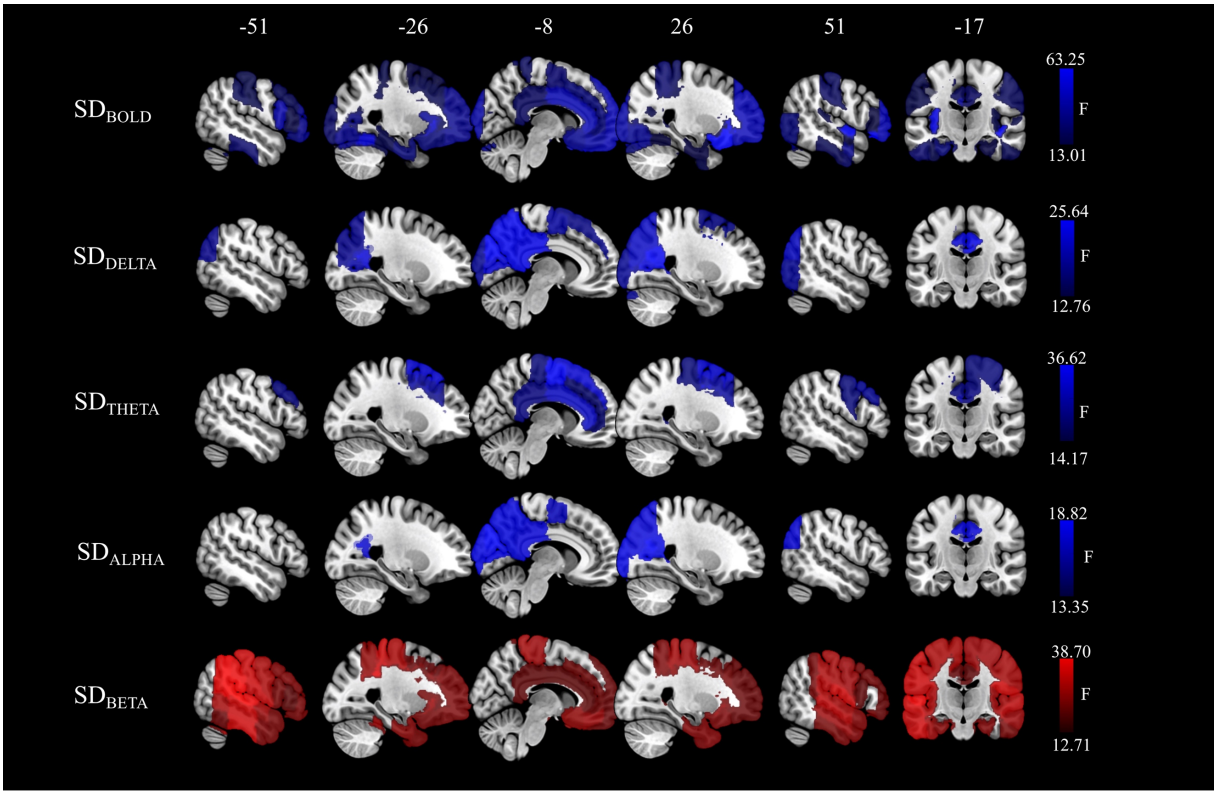

Figure 3. Spatial maps of significant sex differences in SD_{BOLD} and SD_{EEG}.
We calculated the standard deviation (SD) of the blood oxygen level dependent (BOLD) signal and of the coarse-grained amplitude envelope of the rsEEG time series for the delta (1–3 Hz), theta (4–8 Hz), alpha (8–12 Hz), and beta (15–25 Hz) frequency bands at the source space. Statistical significance was determined using 2x2 ANOVAs corrected for multiple comparisons by false discovery rates (FDR; Benjamini and Hochberg, 1995). Light blue indicates that the brain signal variability was higher in male subjects as compared to female subjects, and yellow indicates the opposite.

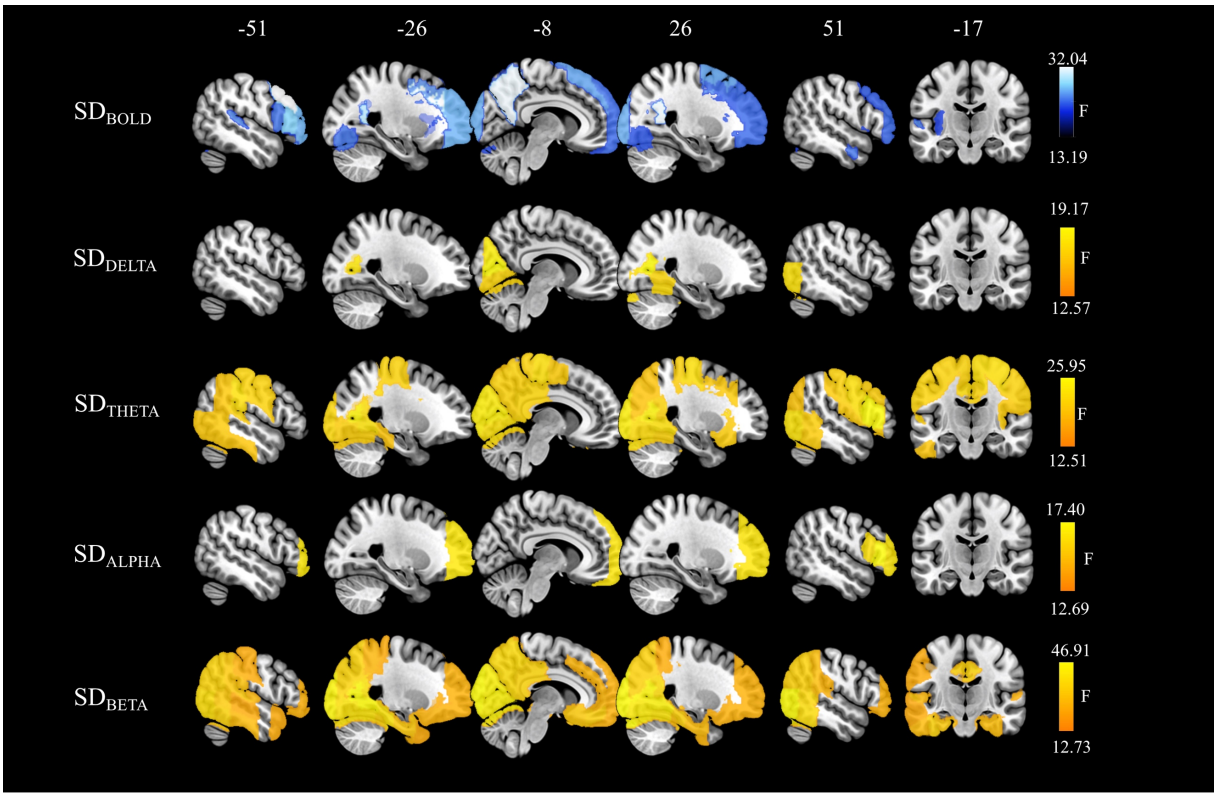

SD_{BOLD} – SD_{EEG} Correlation. The correlation coefficient of pairwise associations for 96 ROIs of SD_{BOLD} with SD_{DELTA}, SD_{THETA}, SD_{ALPHA}, and SD_{BETA} ranged in younger adults from rho=-0.200 to rho=0.223 (Figure 4A, Supplementary Table 6) and in older adults from rho=0.386 to rho=0.349 (Figure 4B, Supplementary Table 7). None of the pairwise associations between SD_{BOLD} and SD_{EEG} remained significant after the correction for multiple comparison corrections. Confirmatory multivariate sparse CCA further showed that correlations between SD_{BOLD} and SD_{EEG} across all subjects were rather low, highly sparse, and non-significant (SD_{DELTA}; r=0.145, p_{perm} =0.750, l_1=0.367; SD_{THETA}; r=0.143, p_{perm}=0.713 l_1=0.7; SD_{ALPHA}; r=0.153, p_{perm}=0.528, l_1=0.1; SD_{BETA}; r=0. 232, p_{perm}=0.096, l_1=0.633).

Figure 4. The distribution of correlation coefficients (rho) for the association between SD_{BOLD} and SD_{EEG} in A) younger (N=135) and B) older (N=54) adults for different frequency bands. The correlations between SD_{BOLD} and SD_{EEG} were tested using pairwise Spearman's rank correlation corrected for multiple comparison by false discovery rates (FDR; Benjamini and Hochberg, 1995).

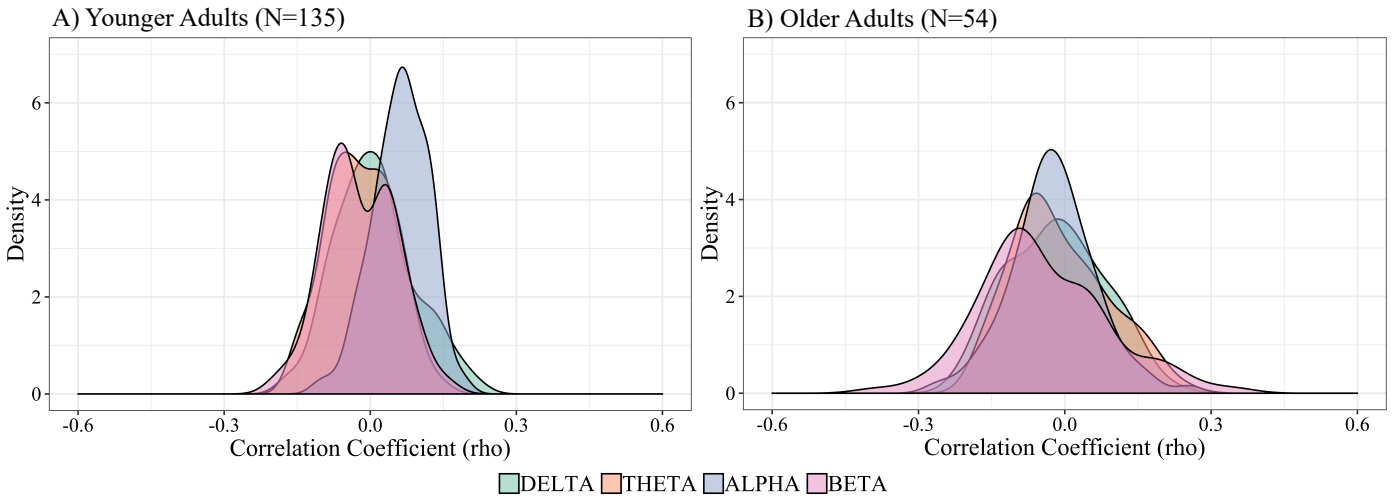

4. Discussion

Comparing healthy younger and older adults, we found widespread variability reductions in BOLD signal as well as in the amplitude envelope of delta, theta, and alpha frequency of rsEEG, whereas increased variability with aging was observed in the beta-band frequency. As a complementary analysis, we also explored sex differences and found that male subjects exhibited higher BOLD signal variability, while the sex differences in the rsEEG variability showed the opposite pattern. There were no significant correlations between hemodynamic (SD_{BOLD}) and electrophysiological (SD_{EEG}) measures of brain signal variability, neither in the younger nor in the older adults. Our results suggest that variability measures of rsfMRI and rsEEG – while both related to aging – are dominated by different physiological origins and relate differently to age and sex.

4.1. BOLD Signal Variability

The first aim of our study was to investigate the effect of age on BOLD signal variability, as measured by SD of spontaneous fluctuations during rsfMRI. Consistent with recent rsfMRI studies demonstrating that BOLD signal variability decreases with age in large-scale networks (Grady and Garrett, 2018; Nomi et al., 2017), we found that older subjects had reduced SD_{BOLD} in temporal and occipital brain regions but also in cortical midline structures like the precuneus, anterior and posterior cingulate cortices, as well as orbitofrontal cortex compared to younger adults. These age-related reductions in BOLD signal variability were thus especially apparent in regions of the Default Mode (DMN) and the Fronto-Parietal Network (FPN). The DMN is an intrinsically correlated network of brain regions, that is particularly active during rest or fixation blocks (Biswal et al., 2010). It reflects the systematic integration of information across the cortex (Margulies et al., 2016) and has been frequently associated with psychological functions like self-referential thought or mind-wandering, and also memory retrieval (Andrews-Hanna et al., 2014; Raichle, 2015). The FPN is involved in cognitive control processes (Spreng et al., 2013), and closely interacts with the DMN, for example during mind-wandering state (Golchert et al., 2017). Previous studies in healthy aging noted that older subjects showed lower connectivity as well as reduced network modularity and functional segregation in DMN and FPN regions (Damoiseaux, 2017; Damoiseaux et al., 2008; Meunier et al., 2009; Petersen et al., 2014). Similarly, an altered functional connectivity in the DMN has been found in different pathologies, for example, in Alzheimer's disease (Greicius et al., 2004) or mild cognitive impairment (Das et al., 2015). One can speculate that decreased BOLD signal variability in the DMN and the FPN,

particularly in the overlapping frontal brain regions, may be related to reduced modularity and integrity in the aging brain, that may reflect functional alterations involved in cognitive processes (Campbell et al., 2012). Therefore, characterizing BOLD signal variability and its transitions in age-related health conditions promises to further our understanding of basic neurocognitive functioning in aging.

In our exploratory analysis of sex differences, we found that male subjects exhibited higher BOLD signal variability in frontal, temporal, and occipital regions than female subjects. Sex-specific differences in brain structure and function have been previously shown (for a review see, Gong et al., 2011; Ruigrok et al., 2014; Sacher et al., 2013). For example, larger total brain volume has been reported in male as compared to female subjects (Gong et al., 2011), whereas higher cerebral blood flow (Gur et al., 1982; Rodriguez et al., 1988) and stronger functional connectivity in the DMN (Tomasi and Volkow, 2012) were found in females than males. Further, a cross-sectional study has demonstrated sex differences in functional connectivity in large-scale resting state networks in aging (Scheinost et al., 2015). Although the relationship between BOLD signal variability and functional connectivity has not been extensively examined, it has been suggested that they may capture similar functional properties (Grady and Garrett, 2018; Leo et al., 2012; Nomi et al., 2017). Assuming this relationship to be genuine, our results correspond to previous studies showing that males have higher functional connectivity strength in occipital, temporal and parietal regions than females (Biswal et al., 2010; Filippi et al., 2012; Ritchie et al., 2018).

4.2.Electrophysiological Signal Variability

Measures of neural variability were derived from rsEEG for several main frequency bands (delta, theta, alpha, beta) as the standard deviation of their amplitude of envelope time series data, analogously to the BOLD signal variability. Multimodal imaging studies have shown that the amplitude envelope of neural oscillatory activity across frequency bands relates to different rsfMRI networks (Brookes et al., 2011; Deligianni et al., 2014), confirming the neurophysiological origin of the resting state networks measured with BOLD fMRI. Additionally, these studies also concluded that different frequency bands can be related to the same functional network, but also differentially to distinct networks (Brookes et al., 2011; Laufs et al., 2006; Mantini et al., 2007; Meyer et al., 2013). For instance, Mantini et. al. (2007) reported that the visual network is associated with all frequency bands with the exclusion of the gamma rhythm, while the sensorimotor network is primarily associated with beta-band oscillations. We found age-dependent EEG signal variability changes within

networks which were associated with more than one frequency band, thus confirming that neurons generating oscillations at different frequencies may contribute to the same network. More precisely, we found age-related reductions in SD_{DELTA} and SD_{ALPHA} mainly in a visual network (including calcarine regions, cuneal cortex, and occipital pole), SD_{THETA} in posterior DMN, while an enhancement of SD_{BETA} was mainly seen in the fronto-temporal and sensorimotor networks. These results align with previous reports of age-dependent changes of electrophysiological activity using spectral power (Dustman et al., 1993; Vlahou et al., 2015), and signal variability (Dustman et al., 1999; Tsvetanov et al., 2015). For instance, age-related decreases of alpha amplitude and alpha band variability (measured by SD of the oscillatory signal) were found in posterior and occipital brain regions (Babiloni et al., 2006; Tsvetanov et al., 2015). Alpha rhythm is a classical EEG hallmark of resting wakefulness (Laufs et al., 2003) that is modulated by thalamo-cortical and cortico-cortical interactions (Bazanova and Vernon, 2014; Goldman et al., 2002; Lopes Da Silva et al., 1997; Moosmann et al., 2003). It has been suggested that the posterior alpha-frequency plays an important role in the top-down control of cortical activation and excitability (Klimesch, 1999). Accordingly, decreased alpha variability in occipital regions might be associated with altered functioning of the cholinergic basal forebrain, affecting thalamo-cortical and cortico-cortical processing. Our finding of an higher fronto-temporal and sensorimotor SD_{BETA} in the elderly is in line with previous findings (Rossiter et al., 2014; Tsvetanov et al., 2015). Aging has previously been associated with an increase in movement-related beta-band attenuation, suggesting an enhanced motor cortex GABAergic inhibitory activity in older individuals (Rossiter et al., 2014). Similarly, beta-band activity is thought to play a key role in signaling maintenance of the status quo of the motor system, despite the absence of movement (Engel and Fries, 2010). Therefore, greater SD_{BETA} in sensorimotor brain regions could be interpreted as a compensatory mechanism to account for a decline of motor performance during aging (Quandt et al., 2016).

In addition to the effect of age on rsEEG signal variability, an exploratory analysis showed sex differences in distinct brain regions and EEG frequencies. More precisely, we found higher SD_{DELTA} in occipital, SD_{THETA} in occipito-temporal, SD_{ALPHA} in frontal, and SD_{BETA} in frontal as well as occipito-temporal brain regions in female compared to male subjects. Previously, higher alpha (Aurlien et al., 2003), theta (Duffy et al., 1993), and beta power (Jaušovec and Jaušovec, 2010; Matsuura et al., 1985; Veldhuizen et al., 1993) have been reported in female relative to male subjects, while the reverse pattern was found in delta power (Zappasodi et al., 2006). Notably, different EEG frequencies were related to distinct hormonal level fluctuations (Becker et al., 1982; Solis-Ortiz et al., 1994). For instance,

reduced absolute theta and alpha power have been reported during the preovulatory phase while increased absolute beta power has been shown during and after the menstrual phase (Solis-Ortiz et al., 1994). Based on this evidence, one could speculate that the sex differences in rsEEG signal variability are related to hormonal variations.

4.3.The Association between BOLD and EEG Variability

We further assessed how neural variability in source-reconstructed rsEEG related to the analogous parameters of BOLD signal variability in rsfMRI using univariate and multivariate correlation analyses. Previously, simultaneous EEG-fMRI studies have shown meaningful relationships between fluctuations in EEG power, frequency, phase, and local BOLD changes (for a review see, Jorge et al., 2014; Ritter and Villringer, 2006). Due to age-related physiological (particularly cardiovascular) alterations in the brain, we expected the relationship between BOLD and EEG signal variability to be stronger in younger than older adults. However, in the present study, both univariate and multivariate analyses showed no significant correlations between SD_{BOLD} and SD_{EEG} neither in the younger nor in the older adults. This finding was supported by the distinct anatomical distributions of age-related changes in BOLD and EEG signal variability, that barely showed a spatial overlap, suggesting different underlying physiological processes. The precise nature of these physiological processes, however, remains speculative, but it seems likely that they include both neuronal and vascular components. The former are likely to be dominant for EEG- and MEG-based variability measures. However, BOLD signal variability seems to reflect both vascular and neural processes (Garrett et al., 2017). The vascular factors in the elderly are, among other things, related to the known morphological changes of blood vessels and metabolic changes with aging which are reflected in CBF (Ances et al., 2009; Martin et al., 1991), $CMRO^2$ (Aanerud et al., 2012), and CVR (Liu et al., 2013). While neuronal components in the rsfMRI BOLD signal are also likely to be relevant (Garrett et al. 2017), the main finding of our study – little correlation with measures of EEG variability – indicates that these neuronal contributions do not dominate BOLD variability measures. While it cannot be excluded that our EEG-based variability measures reflect different aspects of neuronal function than BOLD variability, given these data, it would be desirable to perform – in future studies – concurrent electrophysiological and vascular neuroimaging for a comprehensive assessment of neuronal as well as vascular factors related to aging.

5. Limitations

There are several limitations of our study: EEG and MRI scans were not recorded simultaneously. Therefore, we could not directly relate the two signals in a cross-correlation analysis. Furthermore, EEG and MRI were performed with different body postures (fMRI; supine, EEG; seated) known to affect brain function, for example, changes in the amplitude of the EEG signal have been related to different body postures presumably due to the shifts in cerebrospinal fluid layer thickness (Rice et al., 2013). Moreover, subjects were instructed to lay or sit calm during the recording and not to think of anything particular. However, the participants' actual mental states at rest cannot be controlled or measured accurately, thereby, there might have been differences between the fMRI and EEG recordings. Yet, resting state measures of EEG (Näpflin et al., 2007) and fMRI (Shehzad et al., 2009; Zuo et al., 2010) have been shown to be reliable within-individuals across time. Thus, it is unlikely that there were systematic differences during resting state due to different timing of EEG and fMRI experiments. Finally, the computation of the source reconstructed rsEEG required the parcellation of the brain into relatively large anatomical ROIs. It could well be that the analysis with a higher spatial resolution (e.g., at the voxel-level) may provide additional insights about brain signal variability.

6. Conclusion

In this study, we report age and sex differences of brain signal variability obtained with rsfMRI and rsEEG from the same subjects. We demonstrate extensive age-related reduction of SD_{BOLD}, SD_{DELTA}, SD_{THETA}, and SD_{ALPHA} mainly in the DMN and the visual network, while a significant increase of SD_{BETA} was seen in fronto-temporal and sensorimotor brain regions. We could not demonstrate significant associations between SD_{BOLD} and SD_{EEG}. Our findings indicate that measurements of BOLD and EEG signal variability, respectively, are likely to stem from different physiological origins and relate differentially to age and sex. While the two types of measurements are thus not interchangeable, it seems, however, plausible that both markers of brain variability may provide complementary information about the aging process.

7. Funding

This research did not receive any specific grant from funding agencies in the public, commercial, or not-for-profit sectors.

8. Acknowledgements

We gratefully acknowledge the Mind-Body- Emotion group at the Max Planck Institute for Human Cognitive and Brain Sciences.

9. References

Aanerud, J., Borghammer, P., Mallar Chakravarty, M., Vang, K., Rodell, A.B., Jónsdottir, K.Y., Møller, A., Ashkanian, M., Vafaee, M.S., Iversen, P., Johannsen, P., Gjedde, A., 2012. Brain energy metabolism and blood flow differences in healthy aging. J. Cereb. Blood Flow Metab. https://doi.org/10.1038/jcbfm.2012.18

Ances, B.M., Liang, C.L., Leontiev, O., Perthen, J.E., Fleisher, A.S., Lansing, A.E., Buxton, R.B., 2009. Effects of aging on cerebral blood flow, oxygen metabolism, and blood oxygenation level dependent responses to visual stimulation. Hum. Brain Mapp. 30, 1120–1132. https://doi.org/10.1002/hbm.20574

Andrews-Hanna, J.R., Smallwood, J., Spreng, R.N., 2014. The default network and self-generated thought: Component processes, dynamic control, and clinical relevance. Ann. N. Y. Acad. Sci. 1316, 29–52. https://doi.org/10.1111/nyas.12360

Armbruster-Genc, D.J.N., Ueltzhoffer, K., Fiebach, C.J., 2016. Brain Signal Variability Differentially Affects Cognitive Flexibility and Cognitive Stability. J. Neurosci. 36, 3978–3987. https://doi.org/10.1523/JNEUROSCI.2517-14.2016

Aurlien, H., Gjerde, I.., Aarseth, J.., Eldøen, G., Karlsen, B., Skeidsvoll, H., Gilhus, N.., 2003. EEG background activity described by a large computerized database. Clin. Neurophysiol. 115, 665–673. https://doi.org/10.1016/j.clinph.2003.10.019

Avants, B.B., Tustison, N.J., Song, G., Cook, P.A., Klein, A., Gee, J.C., 2011. A reproducible evaluation of ANTs similarity metric performance in brain image registration. Neuroimage 54, 2033–2044. https://doi.org/10.1016/j.neuroimage.2010.09.025

Babayan, A., Erbey, M., Kumral, D., Reinelt, J.D., Reiter, A.M.F., Röbbig, J., Schaare, H.L., Uhlig, M., Anwander, A., Bazin, P.-L., Horstmann, A., Lampe, L., Nikulin, V. V., Okon-Singer, H., Preusser, S., Pampel, A., Rohr, C.S., Sacher, J., Thöne-Otto, A., Trapp, S., Nierhaus, T., Altmann, D., Arelin, K., Blöchl, M., Bongartz, E., Breig, P., Cesnaite, E., Chen, S., Cozatl, R., Czerwonatis, S., Dambrauskaite, G., Dreyer, M., Enders, J., Engelhardt, M., Fischer, M.M., Forschack, N., Golchert, J., Golz, L., Guran, C.A., Hedrich, S., Hentschel, N., Hoffmann, D.I., Huntenburg, J.M., Jost, R., Kosatschek, A., Kunzendorf, S., Lammers, H., Lauckner, M.E., Mahjoory, K., Kanaan, A.S., Mendes, N., Menger, R., Morino, E., Näthe, K., Neubauer, J., Noyan, H., Oligschläger, S., Panczyszyn-Trzewik, P., Poehlchen, D., Putzke, N., Roski, S., Schaller, M.-C., Schieferbein, A., Schlaak, B., Schmidt, R., Gorgolewski, K.J., Schmidt, H.M., Schrimpf, A., Stasch, S., Voss, M., Wiedemann, A., Margulies, D.S., Gaebler, M., Villringer, A., 2019. A mind-brain-body dataset of MRI, EEG, cognition, emotion, and peripheral

physiology in young and old adults. Sci. Data 6, 180308. https://doi.org/10.1038/sdata.2018.308

Babiloni, C., Binetti, G., Cassarino, A., Dal Forno, G., Del Percio, C., Ferreri, F., Ferri, R., Frisoni, G., Galderisi, S., Hirata, K., Lanuzza, B., Miniussi, C., Mucci, A., Nobili, F., Rodriguez, G., Romani, G.L., Rossini, P.M., Forno, G.D., Percio, C. Del, Ferreri, F., Ferri, R., Frisoni, G., Galderisi, S., Hirata, K., Lanuzza, B., Miniussi, C., Mucci, A., Nobili, F., Rodriguez, G., Romani, G.L., Rossini, P.M., 2006. Sources of cortical rhythms in adults during physiological aging: A multicentric EEG study. Hum. Brain Mapp. 27, 162–172. https://doi.org/10.1002/hbm.20175

Bazanova, O.M., Vernon, D., 2014. Interpreting EEG alpha activity. Neurosci. Biobehav. Rev. 44, 94–110. https://doi.org/10.1016/j.neubiorev.2013.05.007

Bazin, P.L., Weiss, M., Dinse, J., Schäfer, A., Trampel, R., Turner, R., 2014. A computational framework for ultra-high resolution cortical segmentation at 7 Tesla. Neuroimage 93, 201–209. https://doi.org/10.1016/j.neuroimage.2013.03.077

Becker, D., Creutzfeldt, O.D., Schwibbe, M., Wuttke, W., 1982. Changes in physiological, eeg and psychological parameters in women during the spontaneous menstrual cycle and following oral contraceptives. Psychoneuroendocrinology 7, 75–90. https://doi.org/10.1016/0306-4530(82)90057-9

Behzadi, Y., Restom, K., Liau, J., Liu, T.T., 2007. A component based noise correction method (CompCor) for BOLD and perfusion based fMRI. Neuroimage 37, 90–101. https://doi.org/10.1016/j.neuroimage.2007.04.042

Bell, A.J., Sejnowski, T.J., 1995. An Information-Maximization Approach to Blind Separation and Blind Deconvolution. Neural Comput. 7, 1129–1159. https://doi.org/10.1162/neco.1995.7.6.1129

Benjamini, Y., Hochberg, Y., 1995. Controlling the False Discovery Rate : A Practical and Powerful Approach to Multiple Testing Author (s): Yoav Benjamini and Yosef Hochberg Source : Journal of the Royal Statistical Society . Series B (Methodological), Vol . 57 , No . 1 Published by : J. R. Stat. Soc. 57, 289–300.

Birn, R.M., Murphy, K., Bandettini, P.A., 2008. The effect of respiration variations on independent component analysis results of resting state functional connectivity. Hum. Brain Mapp. 29, 740–750. https://doi.org/10.1002/hbm.20577

Biswal, B.B., Mennes, M., Zuo, X.-N., 2010. Toward discovery science of human brain function. Proc. Natl. Acad. Sci. U. S. A. 107, 4734–4739. https://doi.org/10.1073/pnas.0911855107

Brookes, M.J., Woolrich, M., Luckhoo, H., Price, D., Hale, J.R., Stephenson, M.C., Barnes, G.R., Smith, S.M., Morris, P.G., 2011. Investigating the electrophysiological basis of resting state networks using magnetoencephalography. Proc. Natl. Acad. Sci. 108, 16783–16788. https://doi.org/10.1073/pnas.1112685108

Burgess, A., Gruzelier, J., 1993. Individual reliability of amplitude distribution in topographical mapping of EEG. Electroencephalogr. Clin. Neurophysiol. 86, 219–223. https://doi.org/10.1016/0013-4694(93)90101-Z

Caballero-Gaudes, C., Reynolds, R.C., 2017. Methods for cleaning the BOLD fMRI signal. Neuroimage 154, 128–149. https://doi.org/10.1016/j.neuroimage.2016.12.018

Cabeza, R., 2001. Cognitive neuroscience of aging: Contributions of functional neuroimaging. Scand. J. Psychol. 42, 277–286. https://doi.org/10.1111/1467-9450.00237

Cabeza, R., Albert, M., Belleville, S., Craik, F.I.M., Duarte, A., Grady, C.L., Lindenberger, U., Nyberg, L., Park, D.C., Reuter-Lorenz, P.A., Rugg, M.D., Steffener, J., Rajah, M.N., 2018. Maintenance, reserve and compensation: the cognitive neuroscience of healthy ageing. Nat. Rev. Neurosci. 19, 701–710. https://doi.org/10.1038/s41583-018-0068-2

Campbell, K.L., Grady, C.L., Ng, C., Hasher, L., 2012. Age differences in the frontoparietal cognitive control network: Implications for distractibility. Neuropsychologia 50, 2212–2223. https://doi.org/10.1016/j.neuropsychologia.2012.05.025

Chang, C., Cunningham, J.P., Glover, G.H., 2009. Influence of heart rate on the BOLD signal: The cardiac response function. Neuroimage 44, 857–869. https://doi.org/10.1016/j.neuroimage.2008.09.029

Chang, C., Liu, Z., Chen, M.C., Liu, X., Duyn, J.H., 2013. EEG correlates of time-varying BOLD functional connectivity. Neuroimage 72, 227–236. https://doi.org/10.1016/j.neuroimage.2013.01.049

Cohen, M.X., 2017. Where Does EEG Come From and What Does It Mean? Trends Neurosci. 40, 208–218. https://doi.org/10.1016/j.tins.2017.02.004

Cox, R.W., 1996. AFNI: Software for Analysis and Visualization of Functional Magnetic Resonance Neuroimages. Comput. Biomed. Res. 29, 162–173. https://doi.org/10.1006/cbmr.1996.0014

D'Esposito, M., Deouell, L.Y., Gazzaley, A., 2003. Alterations in the BOLD fMRI signal with ageing and disease: a challenge for neuroimaging. Nat. Rev. Neurosci. 4, 863–872. https://doi.org/10.1038/nrn1246

Damoiseaux, J.S., 2017. Effects of aging on functional and structural brain connectivity. Neuroimage 160, 32–40. https://doi.org/10.1016/j.neuroimage.2017.01.077

Damoiseaux, J.S., Beckmann, C.F., Arigita, E.J.S., Barkhof, F., Scheltens, P., Stam, C.J., Smith, S.M., Rombouts, S.A.R.B., 2008. Reduced resting-state brain activity in the "default network" in normal aging. Cereb. Cortex 18, 1856–1864. https://doi.org/10.1093/cercor/bhm207

Das, S.R., Pluta, J., Mancuso, L., Kliot, D., Yushkevich, P.A., Wolk, D.A., 2015. Anterior and posterior MTL networks in aging and MCI. Neurobiol. Aging 36, S141–S150. https://doi.org/10.1016/j.neurobiolaging.2014.03.041

Deligianni, F., Centeno, M., Carmichael, D.W., Clayden, J.D., 2014. Relating resting-state fMRI and EEG whole-brain connectomes across frequency bands. Front. Neurosci. 8, 1–16. https://doi.org/10.3389/fnins.2014.00258

Delorme, A., Makeig, S., 2004. EEGLAB: an open sorce toolbox for analysis of single-trail EEG dynamics including independent component anlaysis. J. Neurosci. Methods 134, 9–21. https://doi.org/10.1016/j.jneumeth.2003.10.009

Desikan, R.S., Ségonne, F., Fischl, B., Quinn, B.T., Dickerson, B.C., Blacker, D., Buckner, R.L., Dale, A.M., Maguire, R.P., Hyman, B.T., Albert, M.S., Killiany, R.J., 2006. An automated labeling system for subdividing the human cerebral cortex on MRI scans into gyral based regions of interest. Neuroimage 31, 968–980. https://doi.org/10.1016/j.neuroimage.2006.01.021

Duffy, F.H., McAnulty, G.B., Albert, M.S., 1993. The pattern of age-related differences in electrophysiological activity of healthy males and females. Neurobiol. Aging 14, 73–84. https://doi.org/10.1016/0197-4580(93)90025-7

Dustman, R.E., Shearer, D.E., Emmerson, R.Y., 1999. Life-span changes in EEG spectral amplitude, amplitude variability and mean frequency. Clin. Neurophysiol. 110, 1399–1409. https://doi.org/10.1016/S1388-2457(99)00102-9

Dustman, R.E., Shearer, D.E., Emmerson, R.Y., 1993. EEG and event-related potentials in normal aging. Prog. Neurobiol. 41, 369–401. https://doi.org/10.1016/0301-0082(93)90005-D

Engel, A.K., Fries, P., 2010. Beta-band oscillations-signalling the status quo? Curr. Opin. Neurobiol. 20, 156–165. https://doi.org/10.1016/j.conb.2010.02.015

Failla, M., Grappiolo, A., Emanuelli, G., Vitale, G., Fraschini, N., Bigoni, M., Grieco, N., Denti, M., Giannattasio, C., Mancia, G., 1999. Sympathetic tone restrains arterial distensibility of healthy and atherosclerotic subjects. J. Hypertens. 17, 1117–1123. https://doi.org/10.1097/00004872-199917080-00011

Farkas, E., Luiten, P.G.M., 2001. Cerebral microvascular pathology in aging and Alzheimer's

disease, Progress in Neurobiology. https://doi.org/10.1016/S0301-0082(00)00068-X

Fernández, A., Zuluaga, P., Abásolo, D., Gómez, C., Serra, A., Méndez, M.A., Hornero, R., 2012. Brain oscillatory complexity across the life span. Clin. Neurophysiol. 123, 2154–2162. https://doi.org/10.1016/j.clinph.2012.04.025

Filippi, M., Valsasina, P., Misci, P., Falini, A., Comi, G., Rocca, M.A., 2012. The Organization of Intrinsic Brain Activity Differs Between Genders : A Resting-State FMRI Study in a Large Cohort of Young Healthy Subjects 000. https://doi.org/10.1002/hbm.21514

Fischl, B., 2012. FreeSurfer. Neuroimage 62, 774–781. https://doi.org/10.1016/j.neuroimage.2012.01.021

Friston, K.J., Williams, S., Howard, R., Frackowiak, R.S.J., Turner, R., 1996. Movement-related effects in fMRI time-series. Magn. Reson. Med. 35, 346–355. https://doi.org/10.1002/mrm.1910350312

Garrett, D.D., Kovacevic, N., McIntosh, A.R., Grady, C.L., 2013a. The modulation of BOLD variability between cognitive states varies by age and processing speed. Cereb. Cortex 23, 684–693. https://doi.org/10.1093/cercor/bhs055

Garrett, D.D., Lindenberger, U., Hoge, R.D., Gauthier, C.J., 2017. Age differences in brain signal variability are robust to multiple vascular controls. Sci. Rep. 7, 10149. https://doi.org/10.1038/s41598-017-09752-7

Garrett, D.D., Nagel, I.E., Preuschhof, C., Burzynska, A.Z., Marchner, J., Wiegert, S., Jungehülsing, G.J., Nyberg, L., Villringer, A., Li, S.-C., Heekeren, H.R., Bäckman, L., Lindenberger, U., 2015. Amphetamine modulates brain signal variability and working memory in younger and older adults. Proc. Natl. Acad. Sci. 112, 7593–7598. https://doi.org/10.1073/pnas.1504090112

Garrett, D.D., Samanez-Larkin, G.R., MacDonald, S.W.S., Lindenberger, U., McIntosh, A.R., Grady, C.L., 2013b. Moment-to-moment brain signal variability: A next frontier in human brain mapping? Neurosci. Biobehav. Rev. 37, 610–624. https://doi.org/10.1016/j.neubiorev.2013.02.015

Geerligs, L., Tsvetanov, K.A., Cam-CAN, Henson, R.N., 2017. Challenges in measuring individual differences in functional connectivity using fMRI: The case of healthy aging. Hum. Brain Mapp. 38, 4125–4156. https://doi.org/10.1002/hbm.23653

Golchert, J., Smallwood, J., Jefferies, E., Seli, P., Huntenburg, J.M., Liem, F., Lauckner, M.E., Oligschläger, S., Bernhardt, B.C., Villringer, A., Margulies, D.S., 2017. Individual variation in intentionality in the mind-wandering state is reflected in the integration of

the default-mode, fronto-parietal, and limbic networks. Neuroimage 146, 226–235. https://doi.org/10.1016/j.neuroimage.2016.11.025

Goldman, R.I., Stern, J.M., Engel, J., Cohen, M.S., 2002. Simultaneous EEG and fMRI of the alpha rhythm. Neuroreport 13, 2487–2492. https://doi.org/10.1097/00001756-200212200-00022

Gonçalves, S.I., De Munck, J.C., Pouwels, P.J.W., Schoonhoven, R., Kuijer, J.P.A., Maurits, N.M., Hoogduin, J.M., Van Someren, E.J.W., Heethaar, R.M., Lopes Da Silva, F.H., 2006. Correlating the alpha rhythm to BOLD using simultaneous EEG/fMRI: Inter-subject variability. Neuroimage 30, 203–213. https://doi.org/10.1016/j.neuroimage.2005.09.062

Gong, G., He, Y., Evans, A.C., 2011. Brain connectivity: Gender makes a difference. Neuroscientist 17, 575–591. https://doi.org/10.1177/1073858410386492

Gorgolewski, K., Burns, C.D., Madison, C., Clark, D., Halchenko, Y.O., Waskom, M.L., Ghosh, S.S., 2011. Nipype: A Flexible, Lightweight and Extensible Neuroimaging Data Processing Framework in Python. Front. Neuroinform. 5, 13. https://doi.org/10.3389/fninf.2011.00013

Grady, C., 2012. The cognitive neuroscience of ageing. Nat. Rev. Neurosci. 13, 491–505. https://doi.org/10.1038/nrn3256

Grady, C.L., Garrett, D.D., 2018. Brain signal variability is modulated as a function of internal and external demand in younger and older adults. Neuroimage 169, 510–523. https://doi.org/10.1016/j.neuroimage.2017.12.031

Grady, C.L., Garrett, D.D., 2014. Understanding variability in the BOLD signal and why it matters for aging. Brain Imaging Behav. https://doi.org/10.1007/s11682-013-9253-0

Greicius, M.D., Srivastava, G., Reiss, A.L., Menon, V., 2004. Default-mode network activity distinguishes Alzheimer's disease from healthy aging: evidence from functional MRI. Proc. Natl. Acad. Sci. U. S. A. 101, 4637–42. https://doi.org/10.1073/pnas.0308627101

Gur, R.C., Gur, R.E., Obrist, W.D., Hungerbuhler, J.P., Younkin, D., Rosen, A.D., Skolnick, B.E., Reivich, M., 1982. Sex and handedness differences in cerebral blood flow during rest and cognitive activity. Science (80-.). 217, 659–661. https://doi.org/10.1126/science.7089587

Haufe, S., Ewald, A., 2016. A Simulation Framework for Benchmarking EEG-Based Brain Connectivity Estimation Methodologies. Brain Topogr. 1–18. https://doi.org/10.1007/s10548-016-0498-y

Hawkes, C.H., Prescott, R.J., 1973. EEG variation in healthy subjects. Electroencephalogr.

Clin. Neurophysiol. 34, 197–199. https://doi.org/10.1016/0013-4694(73)90048-5

Huang, Y., Parra, L.C., Haufe, S., 2016. The New York Head—A precise standardized volume conductor model for EEG source localization and tES targeting. Neuroimage 140, 150–162. https://doi.org/10.1016/j.neuroimage.2015.12.019

Hudetz, A.G., Biswal, B.B., Shen, H., Lauer, K.K., Kampine, J.P., 1998. Spontaneous Fluctuations in Cerebral Oxygen Supply. Springer, Boston, MA, pp. 551–559. https://doi.org/10.1007/978-1-4615-4863-8_66

Jaušovec, N., Jaušovec, K., 2010. Resting brain activity: Differences between genders. Neuropsychologia 48, 3918–3925. https://doi.org/10.1016/j.neuropsychologia.2010.09.020

Jenkinson, M., Beckmann, C.F., Behrens, T.E.J., Woolrich, M.W., Smith, S.M., 2012. Fsl. Neuroimage 62, 782–790. https://doi.org/10.1016/j.neuroimage.2011.09.015

Jorge, J., Van der Zwaag, W., Figueiredo, P., 2014. EEG-fMRI integration for the study of human brain function. Neuroimage 102, 24–34. https://doi.org/10.1016/j.neuroimage.2013.05.114

Jurcak, V., Tsuzuki, D., Dan, I., 2007. 10/20, 10/10, and 10/5 systems revisited: Their validity as relative head-surface-based positioning systems. Neuroimage 34, 1600–1611. https://doi.org/10.1016/j.neuroimage.2006.09.024

Kielar, A., Deschamps, T., Chu, R.K.O., Jokel, R., Khatamian, Y.B., Chen, J.J., Meltzer, J.A., 2016. Identifying dysfunctional cortex: Dissociable effects of stroke and aging on resting state dynamics in MEG and fmri. Front. Aging Neurosci. 8. https://doi.org/10.3389/fnagi.2016.00040

Klimesch, W., 1999. EEG alpha and theta oscillations reflect cognitive and memory performance: A review and analysis. Brain Res. Rev. 29, 169–195. https://doi.org/10.1016/S0165-0173(98)00056-3

Labrenz, F., Ferri, F., Wrede, K., Forsting, M., Schedlowski, M., Engler, H., Elsenbruch, S., Benson, S., Costantini, M., 2018. Altered temporal variance and functional connectivity of BOLD signal is associated with state anxiety during acute systemic inflammation. Neuroimage 184, 916–924. https://doi.org/10.1016/j.neuroimage.2018.09.056

Laufs, H., Kleinschmidt, A., Holt, J.L., Elfont, R., Krams, M., Paul, J.S., Krakow, K., 2006. Where the BOLD signal goes when alpha EEG leaves. Neuroimage 31, 1408–1418. https://doi.org/10.1016/j.neuroimage.2006.02.002

Laufs, H., Krakow, K., Sterzer, P., Eger, E., Beyerle, A., Kleinschmidt, A., 2003. Electroencephalographic signatures of attentional and cognitive default modes in

spontaneous brain activity fluctuations at rest 100.

Leo, A., Bernardi, G., Handjaras, G., Bonino, D., Ricciardi, E., Pietrini, P., 2012. Increased BOLD Variability in the Parietal Cortex and Enhanced Parieto-Occipital Connectivity during Tactile Perception in Congenitally Blind Individuals. Neural Plast. 2012, 1–8. https://doi.org/10.1155/2012/720278

Lipsitz, L.A., Goldberger, A.L., 1992. Loss of 'Complexity' and Aging: Potential Applications of Fractals and Chaos Theory to Senescence. JAMA J. Am. Med. Assoc. 267, 1806–1809. https://doi.org/10.1001/jama.1992.03480130122036

Liu, P., Hebrank, A.C., Rodrigue, K.M., Kennedy, K.M., Section, J., Park, D.C., Lu, H., 2013. Age-related differences in memory-encoding fMRI responses after accounting for decline in vascular reactivity. Neuroimage 78, 415–425. https://doi.org/10.1016/j.neuroimage.2013.04.053

Liu, T.T., 2013. Neurovascular factors in resting-state functional MRI. Neuroimage 80, 339–348. https://doi.org/10.1016/j.neuroimage.2013.04.071

Logothetis, N.K., 2008. What we can do and what we cannot do with fMRI. Nature 453, 869–878. https://doi.org/10.1038/nature06976

Logothetis, N.K., Wandell, B.A., 2004. Interpreting the BOLD Signal. Annu. Rev. Physiol. 66, 735–769. https://doi.org/10.1146/annurev.physiol.66.082602.092845

Lopes Da Silva, F.H., Pijn, J.P., Velis, D., Nijssen, P.C.G., 1997. Alpha rhythms: Noise, dynamics and models. Int. J. Psychophysiol. 26, 237–249. https://doi.org/10.1016/S0167-8760(97)00767-8

Lopez-Larson, M.P., Anderson, J.S., Ferguson, M.A., Yurgelun-Todd, D., 2011. Local brain connectivity and associations with gender and age. Dev. Cogn. Neurosci. 1, 187–197. https://doi.org/10.1016/j.dcn.2010.10.001

Maltez, J., Hyllienmark, L., Nikulin, V. V., Brismar, T., 2004. Time course and variability of power in different frequency bands of EEG during resting conditions. Neurophysiol. Clin. 34, 195–202. https://doi.org/10.1016/j.neucli.2004.09.003

Mantini, D., Perrucci, M.G., Del Gratta, C., Romani, G.L., Corbetta, M., 2007. Electrophysiological signatures of resting state networks in the human brain. Proc. Natl. Acad. Sci. 104, 13170–13175. https://doi.org/10.1073/pnas.0700668104

Margulies, D.S., Ghosh, S.S., Goulas, A., Falkiewicz, M., Huntenburg, J.M., Langs, G., Bezgin, G., Eickhoff, S.B., Castellanos, F.X., Petrides, M., Jefferies, E., Smallwood, J., 2016. Situating the default-mode network along a principal gradient of macroscale cortical organization. Proc. Natl. Acad. Sci. 113, 12574–12579.

https://doi.org/10.1073/pnas.1608282113

Martin, J., Friston, K.J., Colebatch, J.G., Frackowiak, R.S.J., Unit, M.R.C.C., Hospital, H., 1991. Decreases in Regional Cerebral Blood Flow with Normal Aging 684–689.

Matsuura, M., Yamamoto, K., Fukuzawa, H., Okubo, Y., Uesugi, H., Moriiwa, M., Kojima, T., Shimazono, Y., 1985. Age development and sex differences of various EEG elements in healthy children and adults - Quantification by a computerized waveform recognition method. Electroencephalogr. Clin. Neurophysiol. 60, 394–406. https://doi.org/10.1016/0013-4694(85)91013-2

McBride, J.C., Zhao, X., Munro, N.B., Smith, C.D., Jicha, G.A., Hively, L., Broster, L.S., Schmitt, F.A., Kryscio, R.J., Jiang, Y., 2014. Spectral and complexity analysis of scalp EEG characteristics for mild cognitive impairment and early Alzheimer's disease. Comput. Methods Programs Biomed. 114, 153–163. https://doi.org/10.1016/j.cmpb.2014.01.019

McDonald, J.H., 2014. Handbook of Biological Statistics. Sparky House Publ. 180–185.

Meunier, D., Achard, S., Morcom, A., Bullmore, E., 2009. Age-related changes in modular organization of human brain functional networks. Neuroimage 44, 715–723. https://doi.org/10.1016/j.neuroimage.2008.09.062

Meyer, M.C., Janssen, R.J., Van Oort, E.S.B., Beckmann, C.F., Barth, M., 2013. The Quest for EEG Power Band Correlation with ICA Derived fMRI Resting State Networks. Front. Hum. Neurosci. 7, 315. https://doi.org/10.3389/fnhum.2013.00315

Moosmann, M., Ritter, P., Krastel, I., Brink, A., Thees, S., Blankenburg, F., Taskin, B., Obrig, H., Villringer, A., 2003. Correlates of alpha rhythm in functional magnetic resonance imaging and near infrared spectroscopy. Neuroimage 20, 145–158. https://doi.org/10.1016/S1053-8119(03)00344-6

Murayama, Y., Bieβmann, F., Logothetis, N.K., Oeltermann, A., Müller, K.-R., Meinecke, F.C., Augath, M., 2010. Relationship between neural and hemodynamic signals during spontaneous activity studied with temporal kernel CCA. Magn. Reson. Imaging 28, 1095–1103. https://doi.org/10.1016/j.mri.2009.12.016

Näpflin, M., Wildi, M., Sarnthein, J., 2007. Test-retest reliability of resting EEG spectra validates a statistical signature of persons. Clin. Neurophysiol. 118, 2519–2524. https://doi.org/10.1016/j.clinph.2007.07.022

Niessing, J., Ebisch, B., Schmidt, K.E., Niessing, M., Singer, W., Galuske, R.A.W., 2005. Neuroscience: Hemodynamic signals correlate tightly with synchronized gamma oscillations. Science (80-.). 309, 948–951. https://doi.org/10.1126/science.1110948

Nomi, J.S., Bolt, T.S., Ezie, C.E.C., Uddin, L.Q., Heller, A.S., 2017. Moment-to-Moment BOLD Signal Variability Reflects Regional Changes in Neural Flexibility across the Lifespan. J. Neurosci. 37, 5539–5548. https://doi.org/10.1523/JNEUROSCI.3408-16.2017

Nomi, J.S., Schettini, E., Voorhies, W., Bolt, T.S., Heller, A.S., Uddin, L.Q., 2018. Resting-State Brain Signal Variability in Prefrontal Cortex Is Associated With ADHD Symptom Severity in Children. Front. Hum. Neurosci. 12, 90. https://doi.org/10.3389/fnhum.2018.00090

Oken, B.S., Chiappa, K.H., 1988. Short-term variability in EEG frequency analysis. Electroencephalogr. Clin. Neurophysiol. 69, 191–198. https://doi.org/10.1016/0013-4694(88)90128-9

Pascual-Marqui, R.D., 2007. Discrete, 3D distributed, linear imaging methods of electric neuronal activity. Part 1: exact, zero error localization.

Petersen, S.E., Savalia, N.K., Chan, M.Y., Park, D.C., Wig, G.S., 2014. Decreased segregation of brain systems across the healthy adult lifespan. Proc. Natl. Acad. Sci. 111, E4997–E5006. https://doi.org/10.1073/pnas.1415122111

Quandt, F., Bönstrup, M., Schulz, R., Timmermann, J.E., Zimerman, M., Nolte, G., Hummel, F.C., 2016. Spectral variability in the aged brain during fine motor control. Front. Aging Neurosci. 8. https://doi.org/10.3389/fnagi.2016.00305

Raichle, M.E., 2015. The Brain's Default Mode Network. Annu. Rev. Neurosci. 38, 433–447. https://doi.org/10.1146/annurev-neuro-071013-014030

Rice, J.K., Rorden, C., Little, J.S., Parra, L.C., 2013. Subject position affects EEG magnitudes. Neuroimage 64, 476–484. https://doi.org/10.1016/j.neuroimage.2012.09.041

Ritchie, S.J., Cox, S.R., Shen, X., Lombardo, M. V., Reus, L.M., Alloza, C., Harris, M.A., Alderson, H.L., Hunter, S., Neilson, E., Liewald, D.C.M., Auyeung, B., Whalley, H.C., Lawrie, S.M., Gale, C.R., Bastin, M.E., McIntosh, A.M., Deary, I.J., 2018. Sex differences in the adult human brain: Evidence from 5216 UK biobank participants. Cereb. Cortex 28, 2959–2975. https://doi.org/10.1093/cercor/bhy109

Ritter, P., Moosmann, M., Villringer, A., 2009. Rolandic alpha and beta EEG rhythms' strengths are inversely related to fMRI-BOLD signal in primary somatosensory and motor cortex. Hum. Brain Mapp. 30, 1168–1187. https://doi.org/10.1002/hbm.20585

Ritter, P., Villringer, A., 2006. Simultaneous EEG-fMRI. Neurosci. Biobehav. Rev. 30, 823–838. https://doi.org/10.1016/j.neubiorev.2006.06.008

Rodriguez, G., Warkentin, S., Risberg, J., Rosadini, G., 1988. Sex differences in regional

cerebral blood flow. J. Cereb. Blood Flow Metab. 8, 783–789. https://doi.org/10.1038/jcbfm.1988.133

Rokem, a, Trumpis, M., Perez, F., 2009. Nitime: time-series analysis for neuroimaging data. Proc. 8th Python Sci. Conf. (SciPy 2009) 1–8.

Rossiter, H.E., Davis, E.M., Clark, E. V., Boudrias, M.H., Ward, N.S., 2014. Beta oscillations reflect changes in motor cortex inhibition in healthy ageing. Neuroimage 91, 360–365. https://doi.org/10.1016/j.neuroimage.2014.01.012

Ruigrok, A.N.V., Salimi-Khorshidi, G., Lai, M.C., Baron-Cohen, S., Lombardo, M. V., Tait, R.J., Suckling, J., 2014. A meta-analysis of sex differences in human brain structure. Neurosci. Biobehav. Rev. 39, 34–50. https://doi.org/10.1016/j.neubiorev.2013.12.004

Sacher, J., Neumann, J., Okon-Singer, H., Gotowiec, S., Villringer, A., 2013. Sexual dimorphism in the human brain: Evidence from neuroimaging. Magn. Reson. Imaging 31, 366–375. https://doi.org/10.1016/j.mri.2012.06.007

Scheeringa, R., Fries, P., Petersson, K.M., Oostenveld, R., Grothe, I., Norris, D.G., Hagoort, P., Bastiaansen, M.C.M., 2011. Neuronal Dynamics Underlying High- and Low-Frequency EEG Oscillations Contribute Independently to the Human BOLD Signal. Neuron 69, 572–583. https://doi.org/10.1016/j.neuron.2010.11.044

Scheinost, D., Finn, E.S., Tokoglu, F., Shen, X., Papademetris, X., Hampson, M., Constable, R.T., 2015. Sex differences in normal age trajectories of functional brain networks. Hum. Brain Mapp. 36, 1524–1535. https://doi.org/10.1002/hbm.22720

Seaquist, E.R., Chen, W., Benedict, L.E., Ugurbil, K., Kwag, J.H., Zhu, X.H., Nelson, C.A., 2007. Insulin reduces the BOLD response but is without effect on the VEP during presentation of a visual task in humans. J. Cereb. Blood Flow Metab. 27, 154–160. https://doi.org/10.1038/sj.jcbfm.9600316

Shehzad, Z., Kelly, A.M.C., Reiss, P.T., Gee, D.G., Gotimer, K., Uddin, L.Q., Lee, S.H., Margulies, D.S., Roy, A.K., Biswal, B.B., Petkova, E., Castellanos, F.X., Milham, M.P., 2009. The Resting Brain: Unconstrained yet Reliable. Cereb. Cortex 19, 2209–2229. https://doi.org/10.1093/cercor/bhn256

Sleimen-Malkoun, R., Perdikis, D., Muller, V., Blanc, J.-L., Huys, R., Temprado, J.-J., Jirsa, V.K., 2015. Brain Dynamics of Aging: Multiscale Variability of EEG Signals at Rest and during an Auditory Oddball Task. eNeuro 2. https://doi.org/10.1523/ENEURO.0067-14.2015

Smits, F.M., Porcaro, C., Cottone, C., Cancelli, A., Rossini, P.M., Tecchio, F., 2016. Electroencephalographic fractal dimension in healthy ageing and Alzheimer's disease.

PLoS One 11, 1–16. https://doi.org/10.1371/journal.pone.0149587

Solis-Ortiz, S., Ramos, J., Arce, C., Guevara, M.A., Corsi-Cabrera, M., 1994. Eeg oscillations during menstrual cycle. Int. J. Neurosci. 76, 279–292. https://doi.org/10.3109/00207459408986010

Speelman, C.P., McGann, M., 2013. How mean is the mean? Front. Psychol. 4, 1–12. https://doi.org/10.3389/fpsyg.2013.00451

Spreng, R.N., Sepulcre, J., Turner, G.R., Stevens, W.D., Schacter, D.L., 2013. Intrinsic Architecture Underlying the Relations among the Default, Dorsal Attention, and Frontoparietal Control Networks of the Human Brain. J. Cogn. Neurosci. 25, 74–86. https://doi.org/10.1162/jocn_a_00281

Steriade, M., 2006. Grouping of brain rhythms in corticothalamic systems. Neuroscience 137, 1087–1106. https://doi.org/10.1016/j.neuroscience.2005.10.029

Thompson, G.J., 2018. Neural and metabolic basis of dynamic resting state fMRI. Neuroimage 180, 448–462. https://doi.org/10.1016/j.neuroimage.2017.09.010

Tibshirani, R., 2011. Regression shrinkage and selection via the lasso: a retrospective. J. R. Stat. Soc. Ser. B (Statistical Methodol. 73, 273–282. https://doi.org/10.1111/j.1467-9868.2011.00771.x

Tomasi, D., Volkow, N.D., 2012. Aging and functional brain networks. Mol. Psychiatry 17, 549–558. https://doi.org/10.1038/mp.2011.81

Tsvetanov, K.A., Henson, R.N.A., Tyler, L.K., Davis, S.W., Shafto, M.A., Taylor, J.R., Williams, N., Cam-Can, Rowe, J.B., 2015. The effect of ageing on fMRI: Correction for the confounding effects of vascular reactivity evaluated by joint fMRI and MEG in 335 adults. Hum. Brain Mapp. 36, 2248–2269. https://doi.org/10.1002/hbm.22768

Vaillancourt, D.E., Newell, K.M., 2002. Changing complexity in human behavior and physiology through aging and disease. Neurobiol Aging 23, 1–11. https://doi.org/10.1016/S0197-4580(02)00052-0

Veldhuizen, R.J., Jonkman, E.J., Poortvliet, D.C.J., 1993. Sex differences in age regression parameters of healthy adults-normative data and practical implications. Electroencephalogr. Clin. Neurophysiol. 86, 377–384. https://doi.org/10.1016/0013-4694(93)90133-G

Villringer, A., Dirnagl, U., 1995. Coupling of brain activity and cerebral blood flow: basis of functional neuroimaging. Cerebrovasc. Brain Metab. Rev. 7, 240—276.

Vlahou, E.L., Thurm, F., Kolassa, I.-T., Schlee, W., 2015. Resting-state slow wave power, healthy aging and cognitive performance. Sci. Rep. 4, 5101.

https://doi.org/10.1038/srep05101

Wang, R., Foniok, T., Wamsteeker, J.I., Qiao, M., Tomanek, B., Vivanco, R.A., Tuor, U.I., 2006. Transient blood pressure changes affect the functional magnetic resonance imaging detection of cerebral activation. Neuroimage 31, 1–11. https://doi.org/10.1016/j.neuroimage.2005.12.004

Witten, D.M., Tibshirani, R., Hastie, T., 2009. A penalized matrix decomposition, with applications to sparse principal components and canonical correlation analysis. Biostatistics 10, 515–534. https://doi.org/10.1093/biostatistics/kxp008

Yang, A.C., Huang, C.C., Yeh, H.L., Liu, M.E., Hong, C.J., Tu, P.C., Chen, J.F., Huang, N.E., Peng, C.K., Lin, C.P., Tsai, S.J., 2013. Complexity of spontaneous BOLD activity in default mode network is correlated with cognitive function in normal male elderly: A multiscale entropy analysis. Neurobiol. Aging 34, 428–438. https://doi.org/10.1016/j.neurobiolaging.2012.05.004

Zappasodi, F., Marzetti, L., Olejarczyk, E., Tecchio, F., Pizzella, V., 2015. Age-related changes in electroencephalographic signal complexity. PLoS One 10, 1–13. https://doi.org/10.1371/journal.pone.0141995

Zappasodi, F., Pasqualetti, P., Tombini, M., Ercolani, M., Pizzella, V., Rossini, P.M., Tecchio, F., 2006. Hand cortical representation at rest and during activation: Gender and age effects in the two hemispheres. Clin. Neurophysiol. 117, 1518–1528. https://doi.org/10.1016/j.clinph.2006.03.016

Zöller, D., Schaer, M., Scariati, E., Padula, M.C., Eliez, S., Van De Ville, D., 2017. Disentangling resting-state BOLD variability and PCC functional connectivity in 22q11.2 deletion syndrome. Neuroimage 149, 85–97. https://doi.org/10.1016/j.neuroimage.2017.01.064

Zuo, X.N., Di Martino, A., Kelly, C., Shehzad, Z.E., Gee, D.G., Klein, D.F., Castellanos, F.X., Biswal, B.B., Milham, M.P., 2010. The oscillating brain: Complex and reliable. Neuroimage 49, 1432–1445. https://doi.org/10.1016/j.neuroimage.2009.09.037

10. Supplementary Material

Supplementary Figure 1. Flowchart of selecting participants from the Mind-Brain-Body study.

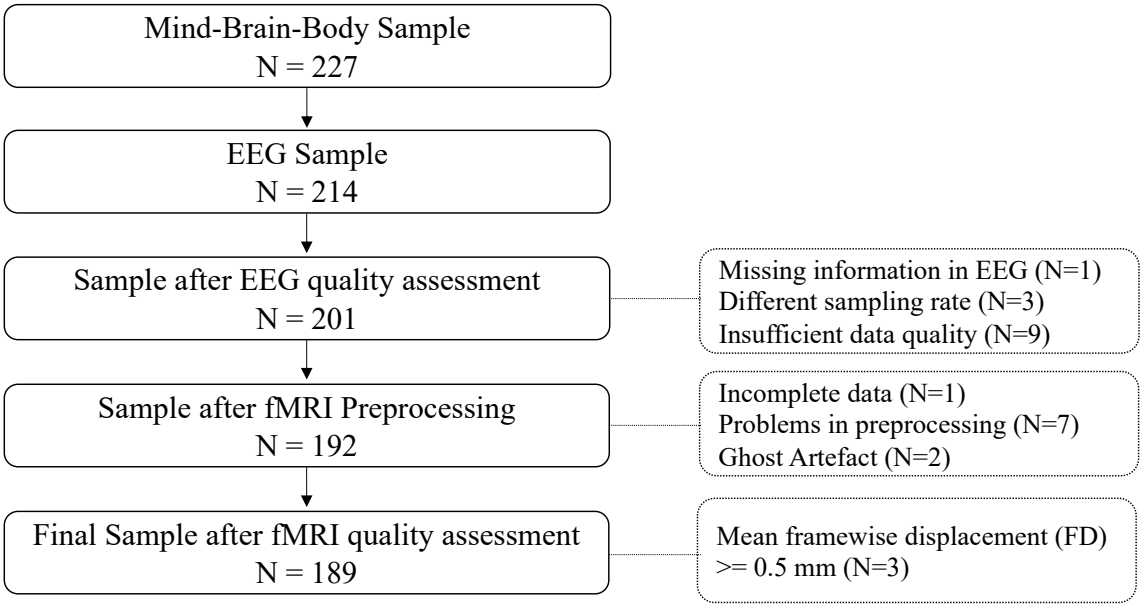

Supplementary Figure 2. Scatter plots showing the distribution of F-values and p-values for the main effect of age group (upper row) and sex (lower row), derived from 2x2 ANOVAs on the brain signal variability values in 96 regions-of-interest (Harvard-Oxford anatomical atlas; Desikan et al., 2006). While x-axes show the F-values for the main effect of age-group, y-axes show the corresponding p-values, corrected for multiple comparisons by false discovery rates(FDR; Benjamini and Hochberg, 1995).

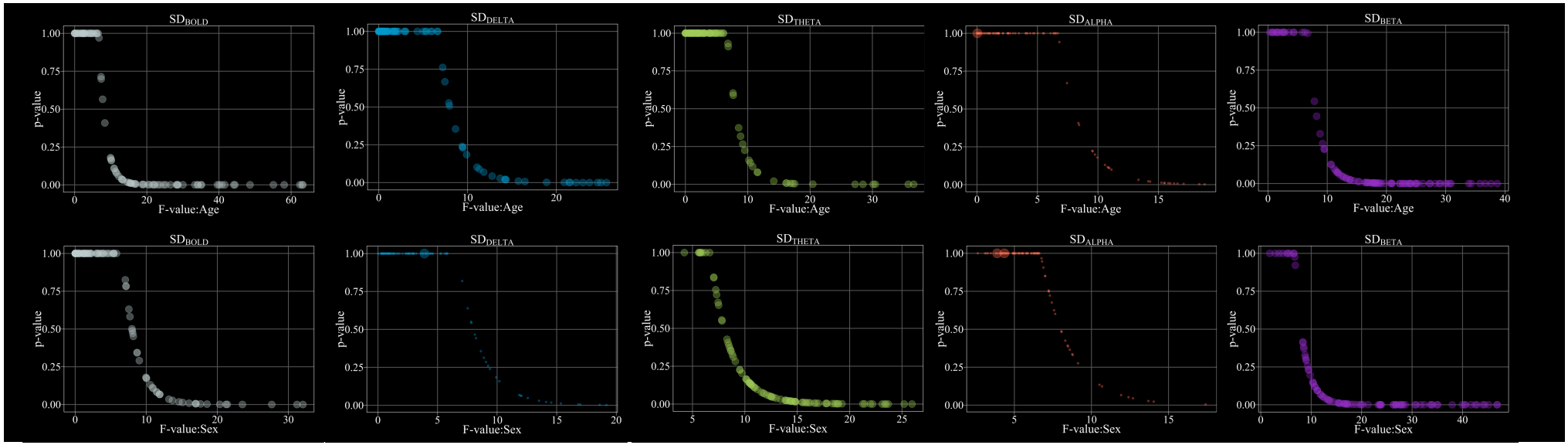

Supplementary Figure 3. Number of brain regions in which brain signal variability as measured by rsfMRI or rsEEG (delta: 1–3 Hz, theta: 4–8 Hz, alpha: 8–12 Hz, beta:15–25 Hz) differed significantly depending on age and sex: 96 region of interests (ROIs), 2x2 ANOVA, corrected for multiple comparisons by false discovery rate (FDR; Benjamini and Hochberg, 1995). Group differences were further examined by Tukey HSD post hoc comparisons. The boxplots show Tukey's post-hoc test results for the differences in brain signal variability measures between age groups (A), and sex (B) respectively.

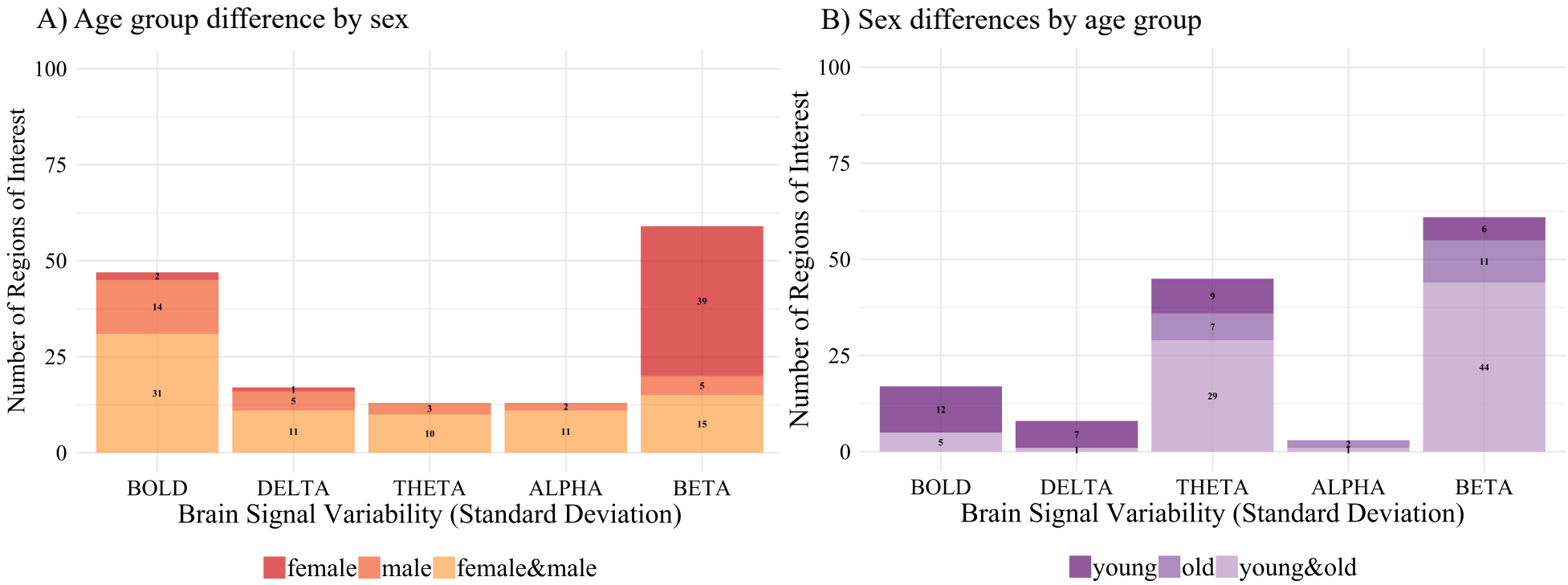

Supplementary Table 1. Table showing the F-values for the main effect of age group (left) and sex (right) for BOLD signal variability (SD_{BOLD}). Statistical significance was determined using 2x2 ANOVAs corrected for multiple comparisons by false discovery rates (FDR; Benjamini and Hochberg, 1995).

ROI	F-value: age
Left Cingulate Gyrus anterior division	48.615
Left Cingulate Gyrus posterior division	20.389
Left Frontal Orbital Cortex	28.551
Left Frontal Pole	34.085
Left Inferior Frontal Gyrus pars opercularis	41.622
Left Inferior Frontal Gyrus pars triangularis	14.852
Left Inferior Temporal Gyrus posterior division	25.290
Left Insular Cortex	58.085
Left Intracalcarine Cortex	30.026
Left Juxtapositional Lobule Cortex formerly Supplementary Motor Cortex	40.124
Left Middle Frontal Gyrus	19.113
Left Occipital Fusiform Gyrus	34.200
Left Occipital Pole	23.057
Left Paracingulate Gyrus	62.433
Left Parahippocampal Gyrus anterior division	28.623
Left Parahippocampal Gyrus posterior division	16.951
Left Postcentral Gyrus	15.551
Left Subcallosal Cortex	22.227
Left Superior Frontal Gyrus	13.411
Left Supracalcarine Cortex	15.271
Left Supramarginal Gyrus anterior division	19.024
Left Temporal Fusiform Cortex posterior division	16.808

ROI	F-value: sex
Left Frontal Operculum Cortex	13.695
Left Frontal Pole	21.401
Left Inferior Frontal Gyrus pars opercularis	16.935
Left Inferior Frontal Gyrus pars triangularis	23.529
Left Insular Cortex	13.187
Left Middle Frontal Gyrus	32.036
Left Occipital Fusiform Gyrus	17.001
Left Planum Temporale	18.550
Left Precuneous Cortex	27.658
Right Frontal Operculum Cortex	17.626
Right Frontal Pole	16.021
Right Middle Frontal Gyrus	15.123
Right Middle Temporal Gyrus anterior division	16.937
Right Occipital Fusiform Gyrus	14.597
Right Occipital Pole	21.222
Right Precuneous Cortex	31.206
Right Superior Frontal Gyrus	20.345

Left Temporal Occipital Fusiform Cortex	55.093
Right Cingulate Gyrus anterior division	44.117
Right Cingulate Gyrus posterior division	21.659
Right Frontal Medial Cortex	39.596
Right Frontal Orbital Cortex	63.259
Right Frontal Pole	44.426
Right Inferior Frontal Gyrus pars triangularis	13.015
Right Inferior Temporal Gyrus anterior division	23.696
Right Inferior Temporal Gyrus posterior division	18.688
Right Insular Cortex	15.497
Right Juxtapositional Lobule Cortex formerly Supplementary Motor Cortex	26.559
Right Lateral Occipital Cortex inferior division	28.214
Right Middle Temporal Gyrus anterior division	33.323
Right Occipital Fusiform Gyrus	35.136
Right Occipital Pole	40.811
Right Paracingulate Gyrus	28.450
Right Parahippocampal Gyrus anterior division	14.644
Right Planum Polare	63.030
Right Planum Temporale	15.649
Right Postcentral Gyrus	20.781
Right Subcallosal Cortex	35.103
Right Superior Parietal Lobule	24.682
Right Superior Temporal Gyrus anterior division	13.131
Right Supracalcarine Cortex	16.332
Right Supramarginal Gyrus anterior division	21.994
Right Temporal Fusiform Cortex anterior division	16.711
Right Temporal Occipital Fusiform Cortex	13.253

Supplementary Table 2. Table showing the F-values for the main effect of age group (left) and sex (right) for EEG signal variability (SD_{DELTA}). Statistical significance was determined using 2x2 ANOVAs corrected for multiple comparisons by false discovery rates (FDR; Benjamini and Hochberg, 1995).

ROI	F value: age
Left Cingulate Gyrus posterior division	21.535
Left Cuneal Cortex	24.636
Left Intracalcarine Cortex	16.454
Left Juxtapositional Lobule Cortex formerly Supplementary Motor Cortex	14.326
Left Lateral Occipital Cortex superior division	13.663
Left Precuneous Cortex	20.890
Left Supracalcarine Cortex	22.222
Right Cingulate Gyrus posterior division	22.989
Right Cuneal Cortex	25.640
Right Intracalcarine Cortex	21.456
Right Juxtapositional Lobule Cortex formerly Supplementary Motor Cortex	15.721
Right Lateral Occipital Cortex inferior division	14.275
Right Lateral Occipital Cortex superior division	18.901
Right Occipital Pole	14.197
Right Precuneous Cortex	23.734
Right Superior Frontal Gyrus	12.769
Right Supracalcarine Cortex	25.020

ROI	F value: sex
Left Cuneal Cortex	14.114
Left Intracalcarine Cortex	15.355
Left Supracalcarine Cortex	16.818
Right Cuneal Cortex	16.985
Right Intracalcarine Cortex	18.605
Right Lateral Occipital Cortex inferior division	14.544
Right Lingual Gyrus	12.575
Right Supracalcarine Cortex	19.167
Right Temporal Occipital Fusiform Cortex	13.512

Supplementary Table 3. Table showing the F-values for the main effect of age group (left) and sex (right) for EEG signal variability (SD_{THETA}). Statistical significance was determined using 2x2 ANOVAs corrected for multiple comparisons by false discovery rates (FDR; Benjamini and Hochberg, 1995).

ROI	F-value: age
Left Cingulate Gyrus anterior division	28.485
Left Cingulate Gyrus posterior division	16.852
Left Juxtapositional Lobule Cortex formerly Supplementary Motor Cortex	35.755
Left Middle Frontal Gyrus	17.237
Left Paracingulate Gyrus	16.139
Left Superior Frontal Gyrus	30.468
Right Cingulate Gyrus anterior division	27.225
Right Cingulate Gyrus posterior division	17.526
Right Juxtapositional Lobule Cortex formerly Supplementary Motor Cortex	36.622
Right Middle Frontal Gyrus	20.439
Right Paracingulate Gyrus	14.178
Right Precentral Gyrus	16.266
Right Superior Frontal Gyrus	30.123

ROI	F-value: sex
Left Angular Gyrus	12.752
Left Cingulate Gyrus posterior division	17.834
Left Cuneal Cortex	21.253
Left Inferior Temporal Gyrus posterior division	13.007
Left Inferior Temporal Gyrus temporooccipital part	13.842
Left Intracalcarine Cortex	23.104
Left Juxtapositional Lobule Cortex formerly Supplementary Motor Cortex	14.819
Left Lateral Occipital Cortex inferior division	13.942
Left Lingual Gyrus	18.89
Left Middle Temporal Gyrus temporooccipital part	14.08
Left Occipital Fusiform Gyrus	14.779
Left Occipital Pole	17.024
Left Parahippocampal Gyrus posterior division	12.582
Left Parietal Operculum Cortex	18.352
Left Planum Temporale	16.806
Left Postcentral Gyrus	16.214
Left Precentral Gyrus	16.055
Left Precuneous Cortex	17.811
Left Supracalcarine Cortex	23.691
Left Supramarginal Gyrus anterior division	18.926

Left Supramarginal Gyrus posterior division	13.417
Left Temporal Occipital Fusiform Cortex	15.509
Right Central Opercular Cortex	14.245
Right Cingulate Gyrus posterior division	16.628
Right Cuneal Cortex	21.429
Right Frontal Operculum Cortex	23.344
Right Frontal Orbital Cortex	14.445
Right Inferior Frontal Gyrus pars opercularis	25.208
Right Inferior Frontal Gyrus pars triangularis	25.954
Right Inferior Temporal Gyrus temporooccipital part	14.395
Right Insular Cortex	14.807
Right Intracalcarine Cortex	22.191
Right Juxtapositional Lobule Cortex formerly Supplementary Motor Cortex	14.315
Right Lateral Occipital Cortex inferior division	19.27
Right Lateral Occipital Cortex superior division	12.508
Right Lingual Gyrus	18.709
Right Middle Frontal Gyrus	14.549
Right Middle Temporal Gyrus temporooccipital part	14.787
Right Occipital Fusiform Gyrus	17.696
Right Occipital Pole	21.974
Right Postcentral Gyrus	15.479
Right Precentral Gyrus	18.576
Right Precuneous Cortex	15.741
Right Supracalcarine Cortex	23.478
Right Supramarginal Gyrus anterior division	13.914
Right Temporal Occipital Fusiform Cortex	15.857

Supplementary Table 4: Table showing the F-values for the main effect of age group (left) and sex (right) for EEG signal variability (SD_{ALPHA}). Statistical significance was determined using 2x2 ANOVAs corrected for multiple comparisons by false discovery rates (FDR; Benjamini and Hochberg, 1995).

ROI	F-value: age
Left Cingulate Gyrus posterior division	15.519
Left Cuneal Cortex	17.085
Left Juxtapositional Lobule Cortex formerly Supplementary Motor Cortex	14.159
Left Precuneous Cortex	14.320
Left Supracalcarine Cortex	16.292
Right Cingulate Gyrus posterior division	15.481
Right Cuneal Cortex	18.827
Right Intracalcarine Cortex	16.574
Right Juxtapositional Lobule Cortex formerly Supplementary Motor Cortex	13.353
Right Lateral Occipital Cortex superior division	15.251
Right Occipital Pole	15.986
Right Precuneous Cortex	15.817
Right Supracalcarine Cortex	18.376

ROI	F-value: sex
Left Frontal Pole	14.036
Right Frontal Pole	13.691
Right Inferior Frontal Gyrus pars opercularis	12.692
Right Inferior Frontal Gyrus pars triangularis	17.399

Supplementary Table 5: Table showing the F-values for the main effect of age group (left) and sex (right) for EEG signal variability (SD_{BETA}). Statistical significance was determined using 2x2 ANOVAs corrected for multiple comparisons by false discovery rates (FDR; Benjamini and Hochberg, 1995).

ROI	F-value: age
Left Angular Gyrus	33.889
Left Central Opercular Cortex	29.092
Left Cingulate Gyrus posterior division	14.001
Left Frontal Medial Cortex	20.640
Left Frontal Operculum Cortex	13.810
Left Frontal Orbital Cortex	16.708
Left Frontal Pole	17.605
Left Heschls Gyrus includes H1 and H2	35.760
Left Inferior Frontal Gyrus pars opercularis	16.834
Left Inferior Frontal Gyrus pars triangularis	12.733
Left Inferior Temporal Gyrus anterior division	17.838
Left Inferior Temporal Gyrus posterior division	30.217
Left Inferior Temporal Gyrus temporooccipital part	15.195
Left Insular Cortex	25.333
Left Middle Frontal Gyrus	18.560
Left Middle Temporal Gyrus anterior division	18.218
Left Middle Temporal Gyrus posterior division	28.902
Left Middle Temporal Gyrus temporooccipital part	23.834
Left Paracingulate Gyrus	13.773
Left Parahippocampal Gyrus anterior division	19.654
Left Parietal Operculum Cortex	37.639
Left Planum Polare	24.914

ROI	F-value: sex
Left Angular Gyrus	27.94
Left Cingulate Gyrus posterior division	27.591
Left Cuneal Cortex	44.014
Left Frontal Medial Cortex	26.259
Left Frontal Orbital Cortex	16.42
Left Frontal Pole	15.711
Left Heschls Gyrus includes H1 and H2	18.317
Left Inferior Temporal Gyrus posterior division	18.946
Left Inferior Temporal Gyrus temporooccipital part	28.281
Left Intracalcarine Cortex	45.176
Left Lateral Occipital Cortex inferior division	32.363
Left Lateral Occipital Cortex superior division	28.676
Left Lingual Gyrus	42.538
Left Middle Temporal Gyrus posterior division	13.19
Left Middle Temporal Gyrus temporooccipital part	23.922
Left Occipital Fusiform Gyrus	33.962
Left Occipital Pole	41.701
Left Paracingulate Gyrus	14.425
Left Parahippocampal Gyrus anterior division	23.759
Left Parahippocampal Gyrus posterior division	33.883
Left Parietal Operculum Cortex	21.278
Left Planum Temporale	23.662

Left Planum Temporale	38.708
Left Postcentral Gyrus	29.919
Left Precentral Gyrus	24.920
Left Subcallosal Cortex	18.873
Left Superior Parietal Lobule	20.882
Left Superior Temporal Gyrus anterior division	20.881
Left Superior Temporal Gyrus posterior division	30.706
Left Supramarginal Gyrus anterior division	34.328
Left Supramarginal Gyrus posterior division	36.668
Left Temporal Fusiform Cortex anterior division	18.248
Left Temporal Fusiform Cortex posterior division	23.363
Left Temporal Pole	17.297
Right Central Opercular Cortex	30.886
Right Cingulate Gyrus anterior division	12.714
Right Cingulate Gyrus posterior division	13.216
Right Frontal Medial Cortex	22.281
Right Frontal Orbital Cortex	17.829
Right Frontal Pole	14.471
Right Heschls Gyrus includes H1 and H2	23.901
Right Inferior Frontal Gyrus pars opercularis	13.248
Right Inferior Temporal Gyrus anterior division	17.982
Right Inferior Temporal Gyrus posterior division	16.913
Right Insular Cortex	23.181
Right Middle Frontal Gyrus	16.461
Right Middle Temporal Gyrus anterior division	22.190
Right Middle Temporal Gyrus posterior division	22.708
Left Postcentral Gyrus	13.534
Left Precuneous Cortex	33.556
Left Subcallosal Cortex	23.546
Left Superior Parietal Lobule	17.175
Left Superior Temporal Gyrus posterior division	12.733
Left Supracalcarine Cortex	46.791
Left Supramarginal Gyrus anterior division	15.331
Left Supramarginal Gyrus posterior division	23.282
Left Temporal Fusiform Cortex anterior division	17.685
Left Temporal Fusiform Cortex posterior division	27.478
Left Temporal Occipital Fusiform Cortex	34.95
Left Temporal Pole	13.448
Right Angular Gyrus	26.753
Right Cingulate Gyrus posterior division	27.907
Right Cuneal Cortex	40.424
Right Frontal Medial Cortex	26.339
Right Frontal Orbital Cortex	15.318
Right Frontal Pole	15.657
Right Inferior Temporal Gyrus temporooccipital part	31.698
Right Intracalcarine Cortex	40.575
Right Lateral Occipital Cortex inferior division	44.382
Right Lateral Occipital Cortex superior division	26.79
Right Lingual Gyrus	39.961
Right Middle Temporal Gyrus temporooccipital part	30.557
Right Occipital Fusiform Gyrus	37.958
Right Occipital Pole	46.91

Right Paracingulate Gyrus	15.398
Right Parahippocampal Gyrus anterior division	18.606
Right Parietal Operculum Cortex	27.257
Right Planum Polare	24.096
Right Planum Temporale	26.151
Right Postcentral Gyrus	24.073
Right Precentral Gyrus	22.804
Right Subcallosal Cortex	20.934
Right Superior Parietal Lobule	17.571
Right Superior Temporal Gyrus anterior division	27.364
Right Superior Temporal Gyrus posterior division	28.260
Right Supramarginal Gyrus anterior division	24.980
Right Supramarginal Gyrus posterior division	16.383
Right Temporal Fusiform Cortex anterior division	18.007
Right Temporal Pole	19.108

Right Paracingulate Gyrus	16.984
Right Parahippocampal Gyrus anterior division	19.682
Right Parahippocampal Gyrus posterior division	26.839
Right Parietal Operculum Cortex	16.684
Right Planum Temporale	17.16
Right Precuneous Cortex	30.788
Right Subcallosal Cortex	23.739
Right Superior Parietal Lobule	13.833
Right Supracalcarine Cortex	42.859
Right Supramarginal Gyrus posterior division	20.224
Right Temporal Fusiform Cortex anterior division	16.612
Right Temporal Fusiform Cortex posterior division	19.912
Right Temporal Occipital Fusiform Cortex	35.103

Supplementary Table 6. Spearman correlation of SD_{BOLD} with SD_{EEG} for each frequency band in young subjects (N=135). None of the pairwise correlations between SD_{BOLD} and SD_{EEG} were statistically significant.

ROI	rho SD_{DELTA}	rho SD_{THETA}	rho SD_{ALPHA}	rho SD_{BETA}
Left Angular Gyrus	0.005	0.015	0.014	0.071
Left Central Opercular Cortex	0.037	0.001	0.076	0.034
Left Cingulate Gyrus, anterior division	-0.090	-0.077	0.091	-0.028
Left Cingulate Gyrus, posterior division	-0.096	-0.048	-0.018	0.042
Left Cuneal Cortex	-0.166	-0.153	-0.040	-0.055
Left Frontal Medial Cortex	-0.009	-0.083	-0.105	-0.100
Left Frontal Operculum Cortex	-0.067	-0.128	0.074	-0.094
Left Frontal Orbital Cortex	0.035	-0.010	0.137	0.107
Left Frontal Pole	0.110	-0.018	-0.029	-0.052
Left Heschl's Gyrus (includes H1 and H2)	-0.019	0.029	0.112	-0.096
Left Inferior Frontal Gyrus, pars opercularis	0.040	-0.082	0.063	-0.091
Left Inferior Frontal Gyrus, pars triangularis	0.031	-0.114	0.064	-0.041
Left Inferior Temporal Gyrus, anterior division	0.035	0.023	0.099	0.012
Left Inferior Temporal Gyrus, posterior division	0.047	0.078	0.116	0.034
Left Inferior Temporal Gyrus, temporooccipital part	0.030	-0.002	0.025	-0.089
Left Insular Cortex	0.023	-0.134	-0.017	-0.077
Left Intracalcarine Cortex	0.018	0.028	0.072	0.032
Left Juxtapositional Lobule Cortex (formerly Supplementary Motor Cortex)	-0.050	-0.099	0.077	0.022
Left Lateral Occipital Cortex, inferior division	-0.048	-0.030	-0.078	-0.077
Left Lateral Occipital Cortex, superior division	-0.062	-0.081	0.018	-0.088
Left Lingual Gyrus	0.131	0.060	-0.022	-0.035
Left Middle Frontal Gyrus	0.041	-0.066	0.131	0.015
Left Middle Temporal Gyrus, anterior division	0.004	-0.063	-0.014	-0.173
Left Middle Temporal Gyrus, posterior division	0.115	0.005	-0.041	-0.029
Left Middle Temporal Gyrus, temporooccipital part	0.072	0.037	0.071	-0.092
Left Occipital Fusiform Gyrus	0.146	0.149	0.115	0.026
Left Occipital Pole	-0.017	0.052	0.036	0.035
Left Paracingulate Gyrus	-0.044	-0.087	-0.012	-0.036
Left Parahippocampal Gyrus, anterior division	0.024	0.021	0.121	0.027
Left Parahippocampal Gyrus, posterior division	-0.086	0.030	0.117	0.162
Left Parietal Operculum Cortex	-0.130	-0.064	0.039	-0.110
Left Planum Polare	0.030	0.018	0.073	-0.004
Left Planum Temporale	-0.066	0.009	0.120	-0.071
Left Postcentral Gyrus	-0.019	-0.032	0.139	-0.060
Left Precentral Gyrus	-0.015	-0.074	0.091	-0.056
Left Precuneous Cortex	-0.029	-0.070	0.107	-0.044

Left Subcallosal Cortex	-0.038	-0.087	0.034	-0.074
Left Superior Frontal Gyrus	-0.108	-0.139	0.027	-0.038
Left Superior Parietal Lobule	0.087	0.041	0.135	-0.084
Left Superior Temporal Gyrus, anterior division	-0.010	-0.074	0.033	0.064
Left Superior Temporal Gyrus, posterior division	-0.059	-0.045	-0.047	-0.087
Left Supracalcarine Cortex	-0.076	-0.071	0.036	0.016
Left Supramarginal Gyrus, anterior division	0.026	-0.060	0.001	-0.057
Left Supramarginal Gyrus, posterior division	-0.005	0.066	0.106	0.043
Left Temporal Fusiform Cortex, anterior division	0.188	0.120	0.051	0.031
Left Temporal Fusiform Cortex, posterior division	0.056	0.052	0.144	0.075
Left Temporal Occipital Fusiform Cortex	0.096	0.094	0.128	0.092
Left Temporal Pole	0.224	0.105	0.152	-0.010
Right Angular Gyrus	-0.010	0.025	0.010	0.046
Right Central Opercular Cortex	0.084	-0.015	0.068	-0.030
Right Cingulate Gyrus, anterior division	-0.079	-0.085	0.062	-0.046
Right Cingulate Gyrus, posterior division	-0.090	-0.048	-0.004	0.021
Right Cuneal Cortex	-0.118	-0.096	0.017	-0.074
Right Frontal Medial Cortex	0.042	-0.043	0.063	-0.050
Right Frontal Operculum Cortex	0.004	-0.017	0.089	-0.075
Right Frontal Orbital Cortex	0.085	-0.024	0.100	-0.032
Right Frontal Pole	0.149	-0.022	0.014	-0.061
Right Heschl's Gyrus (includes H1 and H2)	-0.085	-0.045	0.065	-0.071
Right Inferior Frontal Gyrus, pars opercularis	-0.020	-0.029	0.127	-0.138
Right Inferior Frontal Gyrus, pars triangularis	-0.047	-0.092	0.061	-0.170
Right Inferior Temporal Gyrus, anterior division	0.013	-0.018	0.058	0.028
Right Inferior Temporal Gyrus, posterior division	0.179	0.070	0.128	-0.048
Right Inferior Temporal Gyrus, temporooccipital part	0.106	0.068	0.177	0.093
Right Insular Cortex	-0.034	-0.087	0.043	-0.054
Right Intracalcarine Cortex	-0.063	-0.121	0.008	-0.065
Right Juxtapositional Lobule Cortex (formerly Supplementary Motor Cortex)	-0.040	-0.142	0.015	-0.049
Right Lateral Occipital Cortex, inferior division	-0.025	0.005	0.081	0.026
Right Lateral Occipital Cortex, superior division	-0.008	-0.037	0.044	-0.113
Right Lingual Gyrus	0.040	0.033	0.058	0.034
Right Middle Frontal Gyrus	-0.167	-0.083	0.063	-0.143
Right Middle Temporal Gyrus, anterior division	0.135	0.049	0.054	-0.113
Right Middle Temporal Gyrus, posterior division	0.002	0.080	0.191	0.060
Right Middle Temporal Gyrus, temporooccipital part	0.026	0.011	0.094	0.049
Right Occipital Fusiform Gyrus	0.095	0.039	0.022	0.007
Right Occipital Pole	0.019	-0.050	0.025	-0.036
Right Paracingulate Gyrus	-0.063	-0.041	0.034	-0.012
Right Parahippocampal Gyrus, anterior division	-0.027	-0.005	0.071	0.102

Right Parahippocampal Gyrus, posterior division	0.020	-0.037	0.037	0.024
Right Parietal Operculum Cortex	-0.066	-0.039	0.124	-0.075
Right Planum Polare	0.186	0.073	0.105	-0.021
Right Planum Temporale	-0.028	-0.043	0.074	0.070
Right Postcentral Gyrus	0.070	0.026	0.133	-0.056
Right Precentral Gyrus	-0.031	-0.047	0.134	-0.040
Right Precuneous Cortex	-0.099	-0.145	0.053	-0.200
Right Subcallosal Cortex	-0.084	-0.086	0.098	0.054
Right Superior Frontal Gyrus	-0.100	-0.158	-0.026	-0.116
Right Superior Parietal Lobule	-0.035	-0.067	0.080	-0.103
Right Superior Temporal Gyrus, anterior division	0.144	0.056	0.050	0.021
Right Superior Temporal Gyrus, posterior division	0.067	0.068	0.064	0.004
Right Supracalcarine Cortex	-0.004	0.049	0.089	0.065
Right Supramarginal Gyrus, anterior division	0.134	0.092	0.116	0.046
Right Supramarginal Gyrus, posterior division	0.058	0.055	0.096	0.052
Right Temporal Fusiform Cortex, anterior division	0.038	-0.019	0.013	0.142
Right Temporal Fusiform Cortex, posterior division	0.012	0.011	0.075	0.103
Right Temporal Occipital Fusiform Cortex	-0.013	0.018	0.115	0.098
Right Temporal Pole	0.135	0.006	0.044	-0.129

*$p_{FDR} < 0.05$; **$p_{FDR} < 0.01$; ***$p_{FDR} < 0.001$, 2-tailed

Supplementary Table 7. Spearman correlation of SD_{BOLD} with SD_{EEG} for each frequency band in old subjects (N=54). None of the pairwise correlations between SD_{BOLD} and SD_{EEG} were statistically significant.

ROI	rho SD_{DELTA}	rho SD_{THETA}	rho SD_{ALPHA}	rho SD_{BETA}
Left Angular Gyrus	-0.118	-0.100	-0.001	-0.192
Left Central Opercular Cortex	0.129	0.132	-0.006	0.204
Left Cingulate Gyrus, anterior division	-0.043	0.175	-0.034	0.010
Left Cingulate Gyrus, posterior division	0.014	-0.077	0.012	-0.301
Left Cuneal Cortex	-0.134	-0.157	-0.096	-0.387
Left Frontal Medial Cortex	-0.165	-0.129	-0.265	0.061
Left Frontal Operculum Cortex	0.173	0.168	0.063	0.029
Left Frontal Orbital Cortex	0.085	0.192	0.020	0.021
Left Frontal Pole	0.038	-0.009	-0.044	-0.080
Left Heschl's Gyrus (includes H1 and H2)	-0.066	-0.152	-0.166	0.027
Left Inferior Frontal Gyrus, pars opercularis	0.039	0.041	-0.039	0.177
Left Inferior Frontal Gyrus, pars triangularis	0.107	0.113	0.033	0.086
Left Inferior Temporal Gyrus, anterior division	0.111	0.153	0.088	0.278
Left Inferior Temporal Gyrus, posterior division	0.072	0.040	-0.035	0.040
Left Inferior Temporal Gyrus, temporooccipital part	0.016	0.074	0.034	-0.066
Left Insular Cortex	0.225	0.042	-0.079	0.026
Left Intracalcarine Cortex	0.102	0.130	0.254	0.172
Left Juxtapositional Lobule Cortex (formerly Supplementary Motor Cortex)	-0.054	-0.175	-0.035	-0.059
Left Lateral Occipital Cortex, inferior division	0.036	-0.027	-0.057	-0.184
Left Lateral Occipital Cortex, superior division	0.130	0.033	0.013	-0.083
Left Lingual Gyrus	-0.181	-0.101	-0.044	-0.130
Left Middle Frontal Gyrus	0.159	0.161	-0.009	-0.008
Left Middle Temporal Gyrus, anterior division	-0.004	0.000	-0.012	0.349
Left Middle Temporal Gyrus, posterior division	-0.007	-0.073	-0.197	0.077
Left Middle Temporal Gyrus, temporooccipital part	0.042	0.203	0.128	0.015
Left Occipital Fusiform Gyrus	0.105	0.118	0.088	0.086
Left Occipital Pole	-0.212	-0.082	0.070	-0.203
Left Paracingulate Gyrus	-0.109	-0.024	-0.042	0.065
Left Parahippocampal Gyrus, anterior division	0.048	0.086	-0.069	-0.146
Left Parahippocampal Gyrus, posterior division	-0.012	0.058	0.062	-0.116
Left Parietal Operculum Cortex	0.151	-0.030	-0.036	-0.101
Left Planum Polare	0.041	0.075	-0.010	0.219
Left Planum Temporale	0.139	0.000	-0.060	0.079
Left Postcentral Gyrus	-0.015	-0.118	-0.082	-0.060
Left Precentral Gyrus	-0.131	-0.007	-0.045	-0.060
Left Precuneous Cortex	0.059	0.007	-0.004	-0.101
Left Subcallosal Cortex	-0.065	-0.078	-0.140	-0.002

Left Superior Frontal Gyrus	-0.020	-0.126	-0.050	0.026
Left Superior Parietal Lobule	-0.075	-0.023	0.028	-0.054
Left Superior Temporal Gyrus, anterior division	0.052	0.140	-0.072	0.148
Left Superior Temporal Gyrus, posterior division	-0.150	0.047	0.002	-0.093
Left Supracalcarine Cortex	-0.004	-0.077	0.181	-0.093
Left Supramarginal Gyrus, anterior division	0.029	0.005	-0.033	0.114
Left Supramarginal Gyrus, posterior division	0.167	0.100	0.090	-0.027
Left Temporal Fusiform Cortex, anterior division	0.045	0.076	-0.059	0.062
Left Temporal Fusiform Cortex, posterior division	-0.052	0.124	0.069	0.182
Left Temporal Occipital Fusiform Cortex	0.089	-0.049	-0.054	-0.100
Left Temporal Pole	0.015	0.073	0.025	0.187
Right Angular Gyrus	-0.015	-0.032	0.063	-0.074
Right Central Opercular Cortex	-0.120	-0.020	-0.063	-0.070
Right Cingulate Gyrus, anterior division	0.027	0.176	0.038	0.036
Right Cingulate Gyrus, posterior division	0.092	-0.058	0.051	-0.256
Right Cuneal Cortex	-0.111	-0.174	0.015	-0.224
Right Frontal Medial Cortex	-0.119	-0.072	-0.060	-0.011
Right Frontal Operculum Cortex	-0.032	-0.015	-0.019	-0.056
Right Frontal Orbital Cortex	-0.018	-0.040	-0.104	0.076
Right Frontal Pole	-0.018	-0.050	-0.095	0.058
Right Heschl's Gyrus (includes H1 and H2)	-0.025	-0.084	-0.079	-0.138
Right Inferior Frontal Gyrus, pars opercularis	-0.102	-0.050	-0.156	-0.094
Right Inferior Frontal Gyrus, pars triangularis	-0.215	-0.062	-0.185	-0.128
Right Inferior Temporal Gyrus, anterior division	0.038	-0.076	-0.097	-0.180
Right Inferior Temporal Gyrus, posterior division	0.069	-0.002	-0.071	-0.128
Right Inferior Temporal Gyrus, temporooccipital part	-0.153	-0.115	-0.171	-0.217
Right Insular Cortex	-0.035	0.031	-0.006	-0.068
Right Intracalcarine Cortex	-0.078	-0.140	-0.117	-0.088
Right Juxtapositional Lobule Cortex (formerly Supplementary Motor Cortex)	-0.013	-0.167	-0.114	-0.135
Right Lateral Occipital Cortex, inferior division	-0.055	-0.088	0.125	0.008
Right Lateral Occipital Cortex, superior division	-0.035	-0.078	0.043	-0.119
Right Lingual Gyrus	-0.180	-0.115	-0.096	-0.149
Right Middle Frontal Gyrus	0.117	0.014	0.102	0.055
Right Middle Temporal Gyrus, anterior division	-0.130	-0.068	-0.120	-0.126
Right Middle Temporal Gyrus, posterior division	-0.030	-0.033	-0.008	0.045
Right Middle Temporal Gyrus, temporooccipital part	-0.008	-0.071	0.010	-0.109
Right Occipital Fusiform Gyrus	0.115	0.249	0.163	0.237
Right Occipital Pole	-0.053	-0.067	0.074	-0.006
Right Paracingulate Gyrus	-0.062	0.123	0.042	-0.085
Right Parahippocampal Gyrus, anterior division	-0.093	-0.061	-0.033	-0.109
Right Parahippocampal Gyrus, posterior division	-0.105	-0.118	-0.103	-0.137

Right Parietal Operculum Cortex	0.105	-0.050	-0.019	-0.072
Right Planum Polare	-0.033	0.050	-0.042	-0.148
Right Planum Temporale	-0.064	-0.135	-0.057	-0.209
Right Postcentral Gyrus	-0.071	0.014	0.047	0.051
Right Precentral Gyrus	0.031	0.027	-0.039	-0.175
Right Precuneous Cortex	0.077	0.071	0.010	-0.035
Right Subcallosal Cortex	0.018	0.044	-0.007	-0.106
Right Superior Frontal Gyrus	-0.159	-0.162	-0.149	-0.156
Right Superior Parietal Lobule	-0.007	0.035	-0.001	-0.063
Right Superior Temporal Gyrus, anterior division	-0.155	-0.045	-0.124	-0.175
Right Superior Temporal Gyrus, posterior division	-0.133	-0.052	-0.127	-0.081
Right Supracalcarine Cortex	-0.131	-0.153	0.138	-0.174
Right Supramarginal Gyrus, anterior division	-0.101	-0.061	-0.078	-0.068
Right Supramarginal Gyrus, posterior division	-0.149	-0.079	-0.022	-0.222
Right Temporal Fusiform Cortex, anterior division	-0.005	0.064	-0.020	-0.041
Right Temporal Fusiform Cortex, posterior division	-0.095	-0.036	0.030	-0.137
Right Temporal Occipital Fusiform Cortex	-0.124	-0.080	0.002	-0.073
Right Temporal Pole	-0.181	-0.112	-0.230	-0.284

*$p_{FDR} < 0.05$; **p_{FDR}